Linköping studies in science and technology. Dissertations.
No. 1516

Modeling for control of centrifugal compressors

Oskar Leufvén

Linköpings universitet
INSTITUTE OF TECHNOLOGY

Department of Electrical Engineering
Linköpings universitet, SE–581 83 Linköping, Sweden

Linköping 2013

Linköping studies in science and technology. Dissertations. No. 1516

Modeling for control of centrifugal compressors
Oskar Leufvén
ISBN 978-91-7519-626-8
ISSN 0345-7524

Oskar Leufvén
oleufven@isy.liu.se
www.vehicular.isy.liu.se
Division of Vehicular Systems
Department of Electrical Engineering
Linköpings universitet
SE–581 83 Linköping
Sweden

The **front cover** illustration shows turbos of different sizes, ranging from a small unit for a high pressure stage application of a two stage series sequentially turbo system and up to a large unit for a heavy duty truck application.
The **rear cover** could symbolize humanities strive toward new goals, where occasionally some guidance is appreciated. Since the "fjäll" in the photo, Helags, contains the southern most glacier of Sweden, the rear cover could also illustrate the need to minimize the environmental footprint of the automotive sector. The rear cover might also simply show the author's family during a ski trip toward the highest peak in Sweden south of the polar circle (1796m), four weeks prior to the thesis print deadline. In either way, picture courtesy of Johan Leufvén.

Typeset with LaTeX 2_ε
Printed by LiU-Tryck, Linköping, Sweden 2013

Abstract

Downsizing and turbocharging of engines provide a way to meet increasing demands for efficiency and performance in the automotive industry. An engine design is a result of compromises, e.g. the selection of charging system, and the trend is to reduce these compromises by increasing system complexity. Models have come to play a central role to handle this rise in complexity, and are used for simulation, system optimization and control synthesis. The models should describe the entire operating range, be capable of extrapolation, be easily parameterizable, and wide cover a range of applications.

A novel compressor model is developed which, in addition to the nominal operation, also covers surge, choke and operation at pressure ratios less than one. The model is based on data from more than 300 compressor maps, measurements from engine test stands, and a surge test stand. The general knowledge gained from the in-depth analysis is condensed in the model equations. The model can be automatically parametrized using a compressor map, is based on static functions for low computational cost, and is shown to extrapolate low speed compressor operation well. Furthermore, it is shown to be applicable to compressors of different size, ranging from small car applications to large heavy duty vehicles. Compressor restriction operation is modeled down to a standstill compressor, and shown to agree well with gas stand measurements. Further, the analysis contributes with new knowledge and models for choking pressure ratio and flow.

A method to automatically determine a turbo map, when the turbo is installed on an engine in an engine test stand is developed. The method can be used to validate manufacturer maps or expand the region covered in a map. An analysis of the limits that an engine installation imposes on the reachable points in the compressor map is performed. The addition of a throttle before the compressor is suggested to increase the reachable map region, and an engine and test cell control structure that can be used to automate the measurements is proposed. Two methods that compensate for the deviation between measured and desired speeds, are proposed and investigated. A gas stand map is compared to the map generated in the engine test stand, and a generally good agreement results.

An experimental analysis of the applicability of the commonly used correction factors, used for estimating compressor performance when the inlet conditions deviate from nominal, is performed. Correction factors are vital, to e.g. estimate turbocharger performance for driving at high altitude or to characterize second stage compressor performance, where the variations in inlet conditions are large. Measurements from an engine test stand and a gas stand show a small but clearly measurable trend, with decreasing compressor pressure ratio for decreasing compressor inlet pressure, for points with equal corrected shaft speed and corrected mass flow. A method that enables measurements to be analyzed with modified corrections is developed. As a result, an adjusted shaft speed correction quantity is proposed, incorporating also the inlet pressure in the shaft speed correction.

Populärvetenskaplig sammanfattning

Nedskalning och turboöverladdning av motorer är ett sätt att möta ökande krav på effektivitet och prestanda. Ett antal kompromisser görs vid motorutvecklingen, där exempelvis motorns maximala effekt avgör turbokompressorns maximala flöde. Kompressorns flödesbredd är begränsad och därför blir tryckuppbyggnadsförmågan på låga motorvarvtal reducerad. Turbon måste vidare rotera med hög hastighet för att öka luftdensiteten, och att accelerera turbon till hög hastighet tar tid, vilket brukar kallas för turbofördröjning. Dessa begränsningar kan hanteras exempelvis genom att sekvensstyrda seriellt kopplade tvåstegsturboaggregat används. Ett mindre aggregat utnyttjas då för lägre motorvarvtal. På högre varvtal övertas överladdningsarbetet av ett större aggregat, och den mindre turbon kopplas förbi. För att hantera den ökade komplexitetsnivån hos överladdningssystem tillämpas modellbaserad reglering, där matematiska modeller för olika delkomponenter av motorn är fundamentala verktyg i konceptutveckling och implementering av regler- och övervakningssystem som hanterar kundernas prestandakrav, samtidigt som låga emissioner och lagkrav säkerställs. Kraven på modellerna är att komponentprestanda beskrivs i alla arbetsområden, parametersättning möjliggörs utifrån tillgänglig data, och god extrapolationsförmåga uppvisas. Vidare bör modellen hantera olika applikationer, exempelvis för turboaggregat från små bil- till stora lastbilsmotorer.

I denna avhandling utvecklas en reglerorienterad modell för turbokompressorn. Modellen hanterar samtliga relevanta arbetsregioner: surge, normalt arbetsområde, samt choke och restriktion. Modellen baseras på kunskap från en djuplodande undersökning av stora mängder mätdata, där slutsatser dragna i undersökningen kondenserats ned i modellekvationerna. Mätdatat innefattar bland annat mer än 300 kompressormappar, data från motortestbänkar och data från en speciellt framtagen surgetestutrustning. Modellens förmåga att beskriva turboaggregat av olika storlek visas vara god, och en bra extrapolationsförmåga till låga turbovarvtal visas. Modellens beskrivning av kompressorarbete vid tryckkvoter under ett, för användning i chokat tillstånd, och för turbovarvtal ned till stillastående modelleras och explicita modeller för detta utvecklas. Modellen implementeras i ett existerande motormedelvärdesmodelleringsramverk, och utökar ramverket med beskrivning av kompressorsurge. Modellen av surge visas vara god, och en ny reglerstrategi för att undvika surge föreslås. Prestandaförbättringen med den nya strategin kvantifieras. Vidare föreslås metoder för att mäta turbomappar för motortestcellsinstallationer, varvid två nya metoder för att justera mätta kompressormappunkter för mindre skillnader mellan önskat korrigerat kompressorvarvtal och uppmätt presenteras. En experimentell undersökning av de fundamentala korrektionsekvationerna som används i kompressormappen presenteras likaså, tillsammans med en förslagen utveckling av korrektionsekvationerna. Påverkan från den föreslagna utvecklingen på fordonsmotorers höghöjdsprestanda kvantifieras. Vikten av korrektionsekvationerna speciellt för tvåstegsturbosystem och höghöjdsbruk visas. En ny metod för att öka marginalen till surgelinjen i en kompressormapp föreslås, och metoder för att undersöka applicerbarheten av metoden visas.

Acknowledgment

Compared to common practice I first and foremost want to express my love for Maya and Isabelle, and thank you for being in my life. I love you both!

I then want to take the opportunity to thank a number of persons, without whom there probably would not have been any thesis. I want to express my gratitude to my friends and family for always making sure that I realize that it is not the entire world that spins and whirls (spoon intended) around turbos. Atheer "Turken" Sam, Robert "Slobb" Kihlberg and Erik Höckerdal are especially acknowledged for just being there.

Karl "Längden" Granström (all chargers on the front cover were hurt in the making of this thesis) is acknowledged for providing impressive length to any discussion, Poolpartys and trips to the small(?) cottage on the west coast. Per "TT" (and, while on it, Berit "denna underbara kvinna") Thyr, Martin "Rävhjielhm" Skoglund, Jonas "Callmertzzsch" Callmer, and Hanna Fager are acknowledged for numerous Torsdagslunchen. Patrik "Pata" Martinsson and Jonas "Eken" Ekerli are acknowledged for our nice MC trips.

My office room mate Christofer Sundström (with correct spelling) is acknowledged for endless discussions on all sorts of topics. Lars Nielsen is greatly acknowledged for letting me join Vehicular Systems, and for providing an environment where research topics can be freely pursued. The rest of the Vehicular Systems group is acknowledged for providing coffee break discussions on topics not necessarily related to turbos.

Andreas Thomasson is acknowledged for proofreading parts of this manuscript, and for being an appreciated research partner. Per Öberg and Erik Frisk are acknowledged for their valuable support with the computer systems. Erik and Gabriella Hellström are acknowledged for making it possible to benefit from the cheap dollar exchange rate, and in the continuation making the rear cover photo possible.

The financial support from the Vinnova industry excellence center LINK-SIC, and the industrial partners are also acknowledged. Johannes Andersen provided me with data during my year in Austria as a masters student, and he later, together with Fredrik Lindström, introduced me to the surge test stand. Fredrik Westin and Ragnar Burenius kindly answered my questions on the two stage data from the gas stand. Anders Lundgren and Anders Andreasson helped me during my weeks in the gas stand. Richard Backman and Jonas Cornelsen were invaluable during the installation of the LNF engine, and the two-stage system. Per-Inge Larsson, Anders Larsson and Henrik Flemmer have given valuable input in various topics. Per Andersson (and I do expect at least one question from you during the public defense of this thesis) has been providing helpful input throughout this entire thesis work, and also during the masters thesis work leading up to the PhD studies.

And last, but, (which is certainly true in this case) as the saying goes, not at all the least, I want to express my deepest gratitude for Lars "Lasse" Eriksson. Without your endless guidance this work would not have been accomplished (and probably never started). Thanks!

Contents

Introduction

1

Introduction

The internal combustion engine has for a long time been the most important prime mover for transportation globally. Even though the internal combustion engine basic design has been around since the late 19th century, it still represents an unbeaten compromise.

> "If a new and in truth better technology emerges, the ones who do not adopt the new technology will die overnight."[†]

A combustion engine is simple in its nature; a mix of fuel and air is combusted, and work is produced by the piston in an operating cycle. The amount of combusted air and fuel controls the amount of work that the piston produces. The piston work has to overcome friction and pumping losses, and by making the engine smaller the losses decrease and engine efficiency thereby increases. To increase engine efficiency in this way is commonly referred to as downsizing. However, downsizing has one important disadvantage; a smaller engine can not induct as much air as a larger one, and is therefore less powerful. The less powerful engine can lead to less customer acceptance. One way to increase the torque of the small engine and thereby regain customer acceptance, is by increasing the air charge density. A higher density increases the air mass that can be aspirated by an engine. The increased mass of air allows an increased fuel mass to be burned, increasing the engine torque. It is outside the scope of this thesis to give a comprehensive summary of basic engine operation and the interested reader is referred to e.g. [170], [78] and [153].

For automotive application, a number of charging systems can be used, e.g. supercharging, pressure wave charging or turbocharging. Turbocharging has become the most commonly used charging system, since it is a reliable and robust system. A turbo utilizes some of the energy in the exhaust gas, otherwise lost to the surroundings.

[†]Free translation from a seminar in Swedish by Per Gillbrand.

There are however some compromises in an engine with a single turbo. One compromise is connected to that the mass flow range of a compressor is limited. The compressor of a single turbo system is sized after the maximum engine power, which is tightly coupled to the maximum mass flow. The limited range then imposes restrictions on the pressure build up for small mass flows, and thereby engine torque at low engine speed. Further, a turbo needs to spin with high rotational speed to increase air density, and due to the turbo inertia it takes time to spin up the turbo. This means that the torque response of a turbocharged engine is slower than an equally powerful naturally aspirated engine, which could also lead to less customer acceptance.

Customer acceptance can then again be regained if the complexity of the charging system is allowed to increase, using e.g. a two stage system. A two stage turbo system combines two differently sized turbo units, where the smaller mass flow range of the smaller turbo, means that pressure can be increased for smaller mass flows. Further, due to the smaller inertia of the smaller turbo, it can be spun up faster and thereby improve the torque response of the engine. The smaller unit can then be bypassed for larger mass flows, where instead the larger turbo is used to supply the charge density needed, see e.g. [93] and [56]. Other studied and used charging systems include e.g. parallel sequential systems, combinations of a mechanical compressor and a turbo, or a system that enables both series and parallel configurations depending on operating point. A brief summary of the most important turbo characteristics, is found in Chapter 2, and the interested reader is referred to e.g. [170], [183], [38] and [9].

The increasingly advanced air charging systems add actuators and components to the engine system. This illustrates that in the process of designing more efficient engines, they are made more flexible to reduce design trade-offs and enable optimization, which adds complexity to the system. Systematic methods are needed to handle the increased complexity, and the model based approach has gained increasing interest in the automotive industry. Model based methods can be used as the foundation for concept development and implementation of control systems, that meet the increased demand for engine performance combined with increasingly stringent emission legislations. The model based approach relies upon models, and to be useful it is vital that the models have good descriptive capabilities over the relevant operating range. The models should be easily parameterizable using available data, and it is desirable that they are also able to describe the operation outside of the range of data that were used in the parametrization process, i.e. to extrapolate. It is also beneficial if a given model handles a wide range of applications, e.g. from a small car sized turbo up to a large heavy duty truck turbo. Turbo data is often measured in gas stands and supplied by the turbo manufacturer. These maps are commonly limited to operation in regions with good component performance. The availability of gas stands in the automotive industry and for researchers can be restricted, while engine test stands are more common. Further, measured turbo characteristic can be affected by installation details, and on engine installations can differ from gas stand installations. Hence, methods to characterize turbo performance on engine installations are beneficial, and can aid in validating and extending manufacturer maps.

1.1 Brief summaries and main contributions of appended papers

This section gives brief summaries and presents the main contributions of the papers included in this thesis.

A mean value engine modeling framework is in Paper 1 [95] extended with surge description capability. The Ellipse compressor model, based on a generalization of an ellipse, is proposed as well as a novel surge controller. The paper contributes with a sensitivity analysis, showing the important characteristics that influence surge properties in an engine. This knowledge is further used in the design of the surge controller, that avoids surge and improves vehicle acceleration performance. The gains for a full throttle acceleration scenario resulting from the improved surge control are quantified.

A method for characterizing turbo performance on engine test stand installations is developed in Paper 2 [96]. The paper contributes with a method for determining turbo performance on engine test bench installations. An engine installation imposes limits on the reachable points in the compressor map, and these limits are highlighted, as well as what they depend on. The novel use of a throttle before the compressor is proposed, enabling the engine and turbo system to span a larger region in the compressor map. The paper contributes with an engine and test cell control structure, that can be used to automate and monitor the measurements by controlling the system to the desired operating points. When measuring a speed line, deviations between measured and desired speed can occur, and two new methods for adjusting the measured points to the correct speed are proposed.

An analysis of the corrections used to scale compressor performance for varying inlet conditions is performed in Paper 3 [98]. A surge avoidance strategy is proposed, showing that a reduction in compressor inlet pressure can increase the surge margin. A method to investigate the applicability of the strategy, that is straight forward and general, is also proposed. An experimental analysis of the correction factors, commonly used to determine compressor performance when inlet conditions deviate from nominal conditions, is performed. As a result, extensions to the commonly used correction equations are proposed. Experimental data from an engine test cell and a gas stand show a small, but clearly measurable trend, with decreasing compressor pressure ratio for decreasing compressor inlet pressure. A novel method is developed, enabling measurements to be analyzed with modified corrections. An adjusted shaft speed correction equation is proposed, incorporating also the compressor inlet pressure in the shaft speed correction.

Paper 4 [100] extends the Ellipse compressor model, capable of normal, surge and choke/restriction description, that was proposed for car applications in Paper 1 and [97], to also cover heavy duty applications. The paper analyzes map properties for a database of 236 maps, discussing and highlighting the data distribution and what a practicing engineer can encounter when working with compressor modeling and parameter estimation. The analysis results in the development of a novel automated model parametrization process. The paper further contributes with an investigation that shows good low speed extrapola-

tion capability of the automatically parametrized extended model.

An experimental analysis and modeling of compressor flow for low pressure ratios, resulting from extensive measurements in a gas stand is presented in Paper 5 [99]. The paper contributes with methods to measure restriction map points in a gas stand, and proposes a systematic method to categorize maps into three types: normal, full, or extended. The paper further contributes with analysis and modeling of compressor operation at high flows and low pressure ratios, and also standstill operation. The Ellipse compressor model is validated as a tool to extrapolate unity pressure ratio flow. The model is exploited to deepen the understanding of compressor flow at unity pressure ratio, resulting in the development of models for this flow. An extension to the Ellipse model is presented, and it is exemplified how the experimental findings can be incorporated into a model that describes the high flow and low pressure ratio operation of centrifugal compressors. The extended model accurately describes the extended maps, also for operation at pressure ratios below unity and under choked conditions.

These five papers form the core of this thesis, and the author has been the principal investigator and main author of all five.

1.2 Other publications by the author

This section summarizes research publications the author have been involved in, that were not included in this thesis.

A Andreas Thomasson, Oskar Leufvén, Ivan Criscuolo and Lars Eriksson, *Modeling and validation of a boost pressure actuation system for a series sequentially turbocharged SI engine*, Accepted for publication in Control Engineering Practice [165]

B Lars Eriksson, Tobias Lindell, Oskar Leufvén, and Andreas Thomasson, *Scalable Component-Based Modeling for Optimizing Engines with Supercharging, E-Boost and Turbocompound Concepts*, 2012, SAE International Journal of Engines [45]

C Lars Eriksson, Tobias Lindell, Oskar Leufvén, and Andreas Thomasson, *Scalable Component-Based Modeling for Optimizing Engines with Supercharging, E-Boost and Turbocompound Concepts*, Technical paper 2012-01-0713, 2012, SAE World Congress, Detroit, USA [46]

D Oskar Leufvén and Lars Eriksson, *Surge and choke capable compressor model*, 2011, IFAC World Congress, Milan, Italy [97]

E Ivan Criscuolo, Oskar Leufvén, Andreas Thomasson, and Lars Eriksson, *Model-based boost pressure control with system voltage disturbance rejection*, 2011, IFAC World Congress, Milan, Italy [33]

F Andreas Thomasson, Lars Eriksson, Oskar Leufvén, and Per Andersson, *Wastegate Actuator Modeling and Model-Based Boost Pressure Control*,

2009, IFAC Workshop on Engine and Powertrain Control, Simulation and Modeling, Paris, France [164]

G Oskar Leufvén, *Compressor Modeling for Control of Automotive Two Stage Turbochargers*, 2010, Licentiate thesis, LiU-TEK-LIC-2010:32, Thesis No. 1463, Linköping University [94]

H Johan Bergström, and Oskar Leufvén, *Surge Modeling and Control of Automotive Turbochargers*, 2007 Masters thesis, LiTH-ISY-EX-07/3999–SE, 1463, Linköping University [14]

The authors contributions to these journal and conference publications are indicated by the author list, where the first author is the main contributor to a publication. In the analysis of the charging system actuator system presented in publications **A** and **E**, the author initialized the project, built the experimental setup and performed the majority of measurements and initial modeling. For publications **B** and **C** the author was contributing with the turbo modeling, and a literature survey of charging concepts. For publication **F** the author was involved in the turbo modeling. The licentiate compilation thesis **G** is based on Paper 1, Paper 2, and earlier versions of publication **D** and Paper 3. During the masters thesis **H**, the author was contributing with the turbo modeling, and the analysis of measurement data.

1.3 Future work

This section briefly presents continuations of this thesis, or research topics that have been found along the way, but that did not gain the deserved attention due to the time constraints.

A turbo consists of two main parts, a compressor and a turbine, and a natural continuation of this thesis is therefore found in its title. To evaluate and validate control oriented turbine models, can be motivated by the development and increased use of twin scroll turbines, mixed flow turbines, and variable geometry turbines.

To investigate and evaluate observer designs based on the developed compressor models is also an interesting continuation. To accurately know the two stage system states, e.g. pressures, temperatures and turbo speeds, is important for a controller. Especially to estimate the shaft speed of the bypassed high pressure stage is an interesting scope. This is important for transients involving a stage switch, where the charging effort is transferred from one of the stages to the other. Further investigation of shaft friction can be motivated by experimental experience from the engine test stand, where the bypassed second stage sometimes stops in friction. For transient two stage control, it is important for the controller to know the shaft speed of the turbos; if the high pressure turbo has stopped or is rotating along in 30 krpm is then vital information.

More measurements of turbo performance for larger variations in inlet conditions, and for more units, compared to the reference conditions, is also a research scope. Such an investigation is also closely related to further investigations of how engine system geometries and properties affect both compressor

and turbine performance, compared to the gas stand measured maps. Also to investigate the applicability of the here proposed centrifugal compressor models to even larger centrifugal compressors for industrial processes, is an interesting continuation.

1.4 Outline

The purpose of the introductory chapters is to introduce the topic, and place the research efforts of this thesis into the research field. An overview of experimental setups used during the thesis work, and a short summary of the appended papers are also given.

The main components making up a turbo: compressor, turbine and center housing with bearings, are introduced in Chapter 2. The goal with the first part of Chapter 2 is to introduce and give an overview of experimental and theoretical studies that not necessarily provide any modeling efforts, but are related to control. Inertia, heat transfer, friction and gas properties are discussed. The turbo performance maps and how they are measured are then presented, with further discussions on characteristic features of a map and phenomena that affect turbo performance. An introduction to model based control, and the mean value engine model framework are then given. This is followed by a short introduction to models of higher dimension than those investigated in this thesis, both for completeness and since higher order modeling has provided inspiration for the models developed in this thesis. Apart from a compressor model, turbine and friction models are needed for full turbo simulations. An overview of available models is presented, and the chapter ends with a presentation of how the turbine and friction models used in this thesis relates to other models.

The entire Chapter 3 then discusses compressor modeling, where compressor operation is divided into three separate regions that are discussed in individual subsections. Surge modeling efforts are presented first, followed by discussions of restriction and choke operation. The normal operation is then exemplified by following an air particle through the compressor stage, using the ideas belonging to the physical modeling family, since this provides an convenient introduction to the underlaying phenomena. The compressor model developed in this thesis belongs to the gray or black box family, which is introduced in the last section. A number of model examples available in the literature are presented, to show the vast flora available to the engineer. The last sub sections then discusses the Ellipse compressor model developed in this thesis, and how it relates to other available models.

Chapter 4 presents two of the experimental setups used for the measurements in this thesis: the engine laboratory at Vehicular Systems and the Saab Trollhättan gas stand. Details on the sensors and measurements systems used are given, along with general information of the test stands.

The five appended papers then make up the rest of the thesis.

2

Turbo

The most common automotive air charging system utilizes a turbo. A turbo consists of a compressor and a turbine on a common shaft, supported by bearings in a center housing. An example of a turbo is shown in Fig. 2.1, where some of the important parts are marked. The housing and bearings are cooled by oil, and commonly also water for the higher exhaust gas temperatures encountered in spark ignition engine applications. The turbine extracts some of the available energy in the exhaust gas stream, and provides a driving torque to the compressor through the common shaft. The compressor is used to increase the intake air density, and thereby the engine power, and the torque needed for the compression process loads the common shaft. The friction also contributes with a loading torque on the shaft. The change in turbo speed ω_{tc} is commonly described using Newton's second law for rotating systems as

$$\frac{d\omega_{tc}}{dt} = \frac{1}{J_{tc}} \left(Tq_t - Tq_c - Tq_{fric} \right) \tag{2.1}$$

where $\omega_{tc}[^{\text{rad}}/_{\text{s}}]$ is the turbo rotational speed, $J_{tc}[\text{kg m}^2]$ the inertia of the rotating components, $Tq_t[\text{Nm}]$ the turbine torque, $Tq_c[\text{Nm}]$ the compressor torque, and $Tq_{fric}[\text{Nm}]$ the torque acting on the shaft due to friction.

This chapter first gives and overview of the compressor, the turbine, and the center housing with bearings and the shaft connecting the compressor and turbine wheel. For each of these turbo components, a summary of theoretical and experimental work available in the literature is presented. Hence the result and conclusions from measurements and high order models will be presented and discussed. Discussions on inertia, unsteady flow, heat transfer, and friction are presented under the center housing section. Some brief comments on gas properties, and commonly used assumptions are also presented. The turbo performance maps are then presented, along with some compressor and

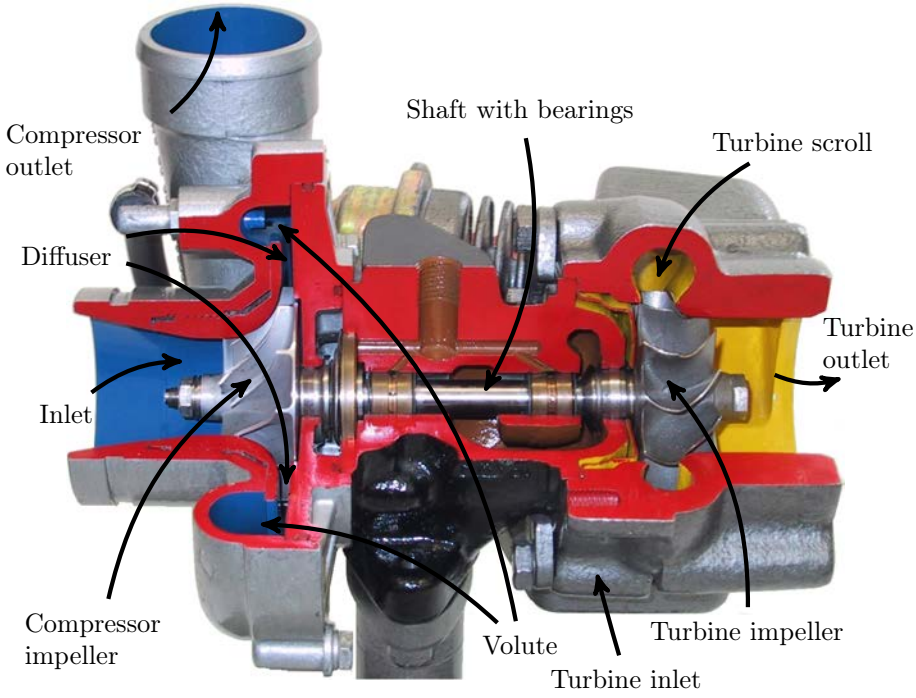

Figure 2.1: Picture of a turbo. The air enters the compressor through the inlet (left) and through the impeller. The heated and pressurized air is then collected in the volute and delivered to the outlet connection (up). The exhaust gas enters the turbine through the turbine inlet (hidden behind the turbo), is lead through the volute into the impeller, where energy is transferred to the impeller vanes and then exits through the outlet (right).

turbine operation characteristics. The next section then presents model based control and mean value engine modeling, followed by a section briefly discussing different model families of various complexity levels.

Modeling efforts related to turbo control are then presented and exemplified for the turbine, and the shaft friction. The presentation focuses on models of a complexity level close to the turbine and friction models used in Papers 1 and 4. The models for Tq_t and Tq_{fric} of (2.1), among others, used in these papers are presented in the last section. The main topic in this thesis, compressor modeling, is given the entire Chapter 3.

For further details and discussions on the turbo, turbo operation or characteristics, the interested reader is referred to the good turbo books that are available in the literature, e.g. [170], [183], [38], [101], [9], and [79].

2.1 Compressor

Centrifugal compressors are used almost exclusively for automotive applications. They are referred to as centrifugal, or radial compressors since the air enters axially, but leaves the compressor impeller in the radial direction. Axial compressors also exist, but are used mainly in e.g. aircraft or power generation applications. Centrifugal will commonly be omitted here for compactness of the following presentation, i.e. the centrifugal compressor will be referred to as only the compressor.

The main components of a compressor are the intake section, the inducer, the impeller, the shroud, the diffuser and the volute, see e.g. [170, 183]. The air flow is first collected in the compressor inlet, which guides the air to the impeller. The inlet casing is essentially a nozzle, used to make the boundary layer blockage thinner and thereby improve impeller performance, see [42, p.781]. The first part of the impeller is commonly referred to as the inducer section. The impeller then consists of many impeller vanes, that rotate at a high velocity. The small turbos making up the second stage of a two stage system can have maximum rotational speeds of 300krpm, and the maximum speed of a larger truck application turbo can be 100krpm. The impeller rotating with high velocity transfers energy to the air flow, and thereby increases the kinetic energy of the air. The air then leaves the compressor impeller in the radial and tangential direction.

Since centrifugal compressors are reaction machines, part of the compression occurs already in the impeller passages, but the main part occurs in the diffuser, see e.g [175, p.3] and [57, p.1466]. Both temperature and pressure increases during compression, even for an ideal compression process. The real pressure increase is however associated with different losses, e.g. flow friction, which increase the rise in temperature even further, and the process is hence not isentropic but polytropic, see e.g. [183, p.60] and [67, p.1344]. While the majority of the diffusion occurs in the diffuser, available kinetic energy can continue to diffuse in the volute, see e.g. [170, p.76], [183, p.55], and[20, p.153].

The diffuser section used for automotive applications is commonly vaneless, since vaned diffusers reduce the compressor flow width, see e.g. [170] and [130, p.131]. The volute works as a diffuser for low mass flow, or as a nozzle at high mass flow, and as neither at the volute design flow rate, see [145, p.118].

A valve can be mounted in close connection to the compressor. This valve is referred to as a surge or recirculation valve, and is used to decrease the pressure after the compressor. The valve opens a connection from the pipe after the compressor to the pipe before, to avoid compressor surge. An example of a closely coupled surge valve built into the compressor scroll is shown in Fig. 2.2. Control of the surge valve is connected to engine performance, and this is studied in Paper 1. For a series sequential two stage system the high pressure stage is commonly equipped with a by-pass valve, which leads compressed air from the first stage around the second stage.

During modeling efforts, different compressor diameters are commonly used. Commonly used diameters are presented in Fig. 2.3. The shaft diameter d_{cs}, the hub diameter d_{ch}, the outer impeller diameter d_{c1} at the inducer section, the exducer diameter d_{c2}, and the compressor diameter d_c are seen. d_c is calculated

Figure 2.2: Compressor scroll with built in recirculation valve or surge valve. For surge control, air is recirculated from the outlet duct through the banana shaped hole at the upper right, through the circular hole close to the banana, and then through internal channels to the compressor inlet which is at the center of the scroll. Control of the surge valve is discussed in Paper 1, and this particular scroll belongs to one of the turbos ran in surge for the measurements of Papers 1 and 4.

as the mean diameter that divides the inlet in two annuli of equal area as

$$d_c = \frac{1}{4}\sqrt{d_{c1}^2 + d_{ch}^2} \tag{2.2}$$

d_c will be commonly used in the compressor modeling in Chapter 3. The hub diameter is mainly given by the nut screwed onto the shaft, which sticks up in the center of the wheel.

The particular wheel design presented in Fig. 2.3 consists of six full impeller vanes, and six splitter blades that starts roughly half the way through the impeller. Splitter blades are commonly used in modern designs, see e.g. [20, p.147]. All twelve blades (both full and splitter) are back-swept at the exducer section of the wheel. The back-sweep angle is usually at least 30^o on modern designs to balance stage stability and impeller stress levels, see e.g. [20, p.142-143] and [170, p.74].

The commercially available single stage turbo designs peripheral rotor speeds, tip speeds, are increasing. A maximum tip speed of $460^{\text{m}}/_{\text{s}}$ is presented as material stress induced limit in [82, p.193], and for aluminum alloys a tip speed limit of $470^{\text{m}}/_{\text{s}}$ is indicated in [170, p.70], and stated to give a maximum pressure ratio limit of roughly 4. In [79, p105], the maximum tip speeds is indicated to be roughly $520^{\text{m}}/_{\text{s}}$, giving a maximum pressure ratio of 4.5. Even higher speeds

Figure 2.3: Example of compressor wheel with six full blades and six splitter blades. The gas enters from above, and leaves in radial direction, and the wheel rotates clockwise. Mitsubishi Heavy Industry (MHI) TD04L-14T compressor wheel used for surge measurement in Papers 1 and 4.

and pressure ratios can be achieved using titanium impellers [79, p105].

In e.g. [20, p.147] and [170, p.57], the vane thickness is said to be typically 0.3% of the d_{c2}, with a lower limit of approximately 0.35mm due to manufacturing processes. The vane thickness limits the vane number, to avoid reducing the compressor eye inlet area, see [170, p.58], while the slip factor indicating the fluid guidance of the wheel, increases with an increased number of blades. The hub thickness is chosen to ensure sufficiently high vibration frequencies, see [20, p.147], and the hub diameter is naturally determined by the shaft diameter, see [170, p.58]. The compressor hub to impeller tip ratio is ≈ 0.2, and the ratio of inducer tip diameter to exducer tip diameter is around 0.5, see [170, p.107]. The peak efficiency generally decreases with a decreased size, since the clearances, and losses are proportionally larger for a smaller design than on a larger, see e.g. [170, p.61] and [80].

Variable geometry compressors exist, see e.g. [170, p.137] and [23], but are not common for automotive applications due to additional cost and packaging constraints. Examples of different variable devices are pre-whirl-generators and variable compressor diffusers, see e.g. [9, p.70-72], [79, p.90], [37, p.184], and [23]. Also modifications to the compressor shroud can be used to widen the stable flow range, see e.g. [52], [9, p.67-70] and [151]. Changing the compressor geometry can give both a reduced surge mass flow, while at the same time not compromise high flow performance apart from the fluid frictional losses associated with the devices, see [37, p.184]. Measurements of compressor performance for different co-swirl are presented in e.g. [173] and [79, p.91].

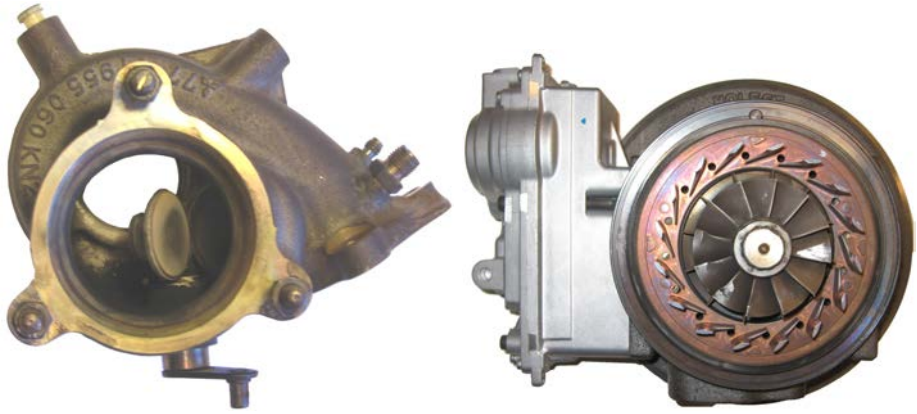

Figure 2.4: Photo into the exhaust side of a turbine housing with WG (left) and a VGT system (right).

2.2 Turbine

While research is being conducted on mixed flow turbines, current automotive applications almost exclusively utilize radial turbines. The radial turbine will therefore here commonly be referred to only as the turbine. The main components making up a turbine, and the occuring losses are presented e.g. in [170] and [79]. The turbine extracts some of the otherwise lost energy from the hot exhaust gas of the combustion engine. The exhaust gas flows through a turbine impeller, where energy is extracted and transferred to the compressor side. Turbines are reaction machines, and a part of the expansion occurs in the stator and the rotor respectively, see e.g. [170] and [57, p.1466]. The degree of reaction of a turbine states how much expansion that occurs in the rotor relative to the total expansion, see e.g. [170, p.151]. As for the compressor, peak turbine efficiency generally decreases with a decrease in size, see [154, p.1].

A waste-gate WG valve is commonly used to control the amount of exhaust gas that flows through the turbine, and thereby the turbine power in automotive petrol engines. The turbines of automotive diesel engines commonly use a variable geometry VGT to control the turbine power, instead of a WG. The VGT actuators effectively change the flow geometry within the turbine using e.g. variable guide vanes, or a variable turbine inlet area, see e.g. [170, p.188-] and [9, p.184-]. The use of VGT as also been studied for petrol engines, see e.g. [4]. A turbine scroll equipped with a built in WG is shown in Fig. 2.4, where also a turbine wheel with VGT guide vanes is shown.

2.3 Center housing

The turbo inertia and friction both have a direct influence on the acceleration of the turbo, see [137, p.187]. But also the heat transfer occurring in turbos have a strong influence on performance and measurements, see e.g. [107, p.227]

and [2].

The bearings of the turbo shaft are mounted in the center housing of the turbo, and are critical components, needed to support the shaft at high speeds. Fluid bearings and ball bearings are commonly used, and are supplied with oil to reduce friction. For small automotive-type turbos, plain bearings in the form or rotating floating bushes are used almost exclusively, see e.g. [170, p.49]. The plain or sleeve bearing is said to give an almost indefinite life, provided clean lubrication fluid, and accepts large out-of-balance loads, vibrations and shocks. However, high oil feeding pressure and flow rates are said to be needed, see [170, p.47]. Ball bearing turbos are also used. The oil supplied, or additional water cooling, is used to cool the turbo.

The different operation of sequential turbocharging systems, compared to a single turbo system, is in [124] said to increase the oil consumption by the turbos. This oil leaks from the center housing through the compressor or turbine. The main parameters affecting the oil consumption are from the experimental study said to be: the bearing house outlet duct oil pressure, the compressor discharge pressure, and the turbine outlet pressure.

In [123, p.377], a 'moment of inertia factor' is introduced. The moment of inertia factor is estimated from known data, and then used to scale inertia for variation in component sizes through a simple multiplication with the relevant radius squared. The effective turbo inertia is in [6, p.122], [19, p.28] and [147] adjusted so that a simulated transient response reflects a measured. Due to the turbo rotor inertia, cyclic torque caused by unsteady operation, only results in small changes in turbo speed (typically $2-5\%$ is stated), see [170, p.182]. However, the angular acceleration can still be large, see [104].

2.3.1 Heat transfer

Good summaries of relevant work surrounding heat transfer modeling of engine exhausts are found in e.g. [89], [43], and [132]. The effect of heat transfer in an automotive turbo system is analyzed in e.g. [3], [26], [10] and [114], and summarized in e.g. [11, p.3]. In [144] the effect on engine volumetric efficiency and turbo lag resulting from turbocharger heat transfer is investigated.

For the turbine, the most of the heat transfer occurs upstream of the rotor, and thus affects the work transfer process, see [11, p.2]. Compared to the turbine, the variation in compressor heat flux with turbine inlet temperature is much less strong, due to the lubricating oil acting as a heat sink, see [10, p.3,9] and [11, p.2]. The compressor external heat transfer is consistently low, but not a negligible fraction of the overall heat transfer. The main effects from the compressor heat transfer is in [26, p.786] said to be the apparent decrease in efficiency due to the additional temperature rise, and also due to the increase in work needed for the compression when the fluid temperature increases. The latter effect is referred to as the reheat effect, see e.g. [38, p.40]. According to predictions of heat flux to the inner surface of the compressor housing, as a function of distance from inlet, negligible heat flux occurs until the leading edge of the impeller, see e.g. [10, p.4] and [11]. An increasing heat flux thereafter results from the compression process, and the largest heat flux occurs for lowest

mass flow, see [10, p.4].

The measured η_c is in [26, p.793] found to only drop slightly with the turbine inlet temperature at higher speeds. For lower speeds, the turbine inlet temperature increasingly affects the measured compressor efficiency. Since the turbine efficiency is commonly estimated from the compressor temperature rise, also unphysical turbine efficiency values can be found for lower speeds, see e.g. [86], [3, p.121] and [145]. The not adiabatic operation of a turbo is further discussed in [26, p.785], where the effect for higher speeds decreases since the work transfer increases. In [31], the heat transfer is said to represent up to 20% of the compressor adiabatic power. The efficiency measured for an electrically driven compressor is, in [5, p.223], reported to be approximately 5% *lower* than comparable data from gas stand tests.

The flow maps are not significantly affected by the heat transfer from turbine to compressor, but the efficiency maps can be, see [86] and [145, p.74]. The measurements in [26, p.793] shows that the compressor pressure rise is unaffected by changing turbine inlet temperature, and it is concluded that the apparent compressor efficiency deficit at low speeds is entirely due to the heat transfer effect. Also the measurements in [150, p.4] show no effect on pressure ratio from heat transfer, and that the largest affect from heat transfer is expected close to surge on low speeds. The heat transfer is also proposed to be modeled and included in the efficiency models, especially for lower speeds, see [3, p.121]. In [150, p.5], a constant heat transfer rate is said to be a reasonable approximation.

The compressor backplate and housing are described as relatively efficient heat exchangers in [112, p.2], due to relatively large area, high temperature drops and low flow rates. A strong correlation between compressor outlet temperature and the compressor casing temperature is shown in [142]. In [10, p.3,11] it is said that while conduction and radiation can be modeled using material thermal properties and data, the convective heat transfer modeling can be challenging. Main heat transfer is said to occur in the diffuser and volute where large surface areas are exposed to the air flow, while heat transfer between the turbine and compressor wheel is said to be neglectable due to the lubricating oil.

Measurements of compressor performance for cases with and without insulation shows that the amount of heat transfer from the compressor through free convection and radiation has almost no effect on the measured compressor efficiency, see [145, p.73,162]. It is further concluded that the compressor can transfer heat to the oil at high turbo speeds. Further, the heat transfer by free convection and radiation from the turbine to the compressor has negligible effect on compressor efficiency. This is said to be due to the relatively small surface area available for convection and radiation compared to the conduction heat paths, and is also supported in [2]. It is stated in [145, p.11, 73] that the low absorptivity, given an emissivity of ≈ 0.63, of the bright compressor casing, reduces the effect of radiation heat transfer. In [142] emissivity levels of 0.1 and 0.9 are assumed for the compressor and turbine casings respectively, and radiation is concluded to be important at small compressor powers.

2.3.2 Friction

An experimental analysis shows the main bearing power losses to be: radial bearing, thrust bearing, wet-oil-cavity (slender shaft area) and seals, see [91, p.3]. In [91], a large oil pressure is said to increase the friction power losses. Further, the thrust bearing losses are the largest contributors to the total friction loss. The turbine power to overcome friction is said to be reduced by half for ball bearings in [172, p.24], and a reduction of 40-80% is presented in [137, p.187]. In [25, p.126], the bearing loss power is assumed to be unchanged in pulsating flow operation. More general pictures of measurements of friction can be found e.g. in [91, p.5] and [77]. Measurements of bearing friction torque vs. oil temperature, and a comparison to manufacturer data is presented in [137, p.194]. Both oil temperature and pressure are linked to friction in [36], using a dedicated torque meter. Friction increases with oil pressure due to that the increased oil flow decreases oil temperature, and thus increases viscosity.

Normally the axial thrust from the compressor and turbine balances each other, see e.g. [170, p.49], however for off-design operation an axial force can be created. Due to the hydrodynamic mode of friction of the thrust bearings, only a weak dependence on the friction forces should result from the loading forces, see e.g. [103] and [77]. The thrust bearing load for a case where no force is created by the compressor wheel is presented in [91]. The turbine side gas velocity is said to create an axial load acting on the thrust bearing, that depends on the gas temperature, due to its effect on the gas density [91, p.6]. Measurements of thrust bearing load can be found in [91, p.6], and models for thrust bearing force and bearing power resulting from variation in compressor inlet guide vane position is presented in [77]. Measurements of friction torque changes due to variations in axial load is compared to manufacturer data in [137, p.196], and it is concluded that a reasonable model for the axial thrust friction should add a friction torque component that is proportional to the magnitude of the axial force.

2.4 Gas properties

A number of fluid properties are commonly assumed to be constant when studying turbo operation. R is treated as constant for temperatures below 1500K in [114], and in [147] both R and c_p are assumed constant. The dynamic viscosity, the thermal conductivity, and the specific heat capacity c_p are assumed to be independent of pressure in [131, p.8], and modeled e.g. in [110]. The variations of c_p with temperature is in [141] said to be important, and the influence of temperature on the specific heat ratio γ_c should be considered when calculating isentropic temperatures. The variation in γ is further said to give rise to $\approx 2.5\%$ of η_c overestimation, and $\approx 5\%$ of η_c underestimation, for the studied temperature range. Variations in humidity are in [141] said to be important in efficiency calculations, only when a very high precision is required. The effect from assuming the humidity to be constant, is quantified to give rise to a underestimation in effective power of $\approx -0.5\%$, with almost negligible effect on the efficiency calculations.

2.5 Turbo performance maps

Turbo performance is usually presented in maps using corrected performance variables. The corrections are important, since the performance maps are otherwise only valid for the conditions under which they were measured. The inlet conditions for the turbine naturally varies with operating points, both in pressure and temperature. But also the compressor inlet conditions vary e.g. with changing ambient conditions (high altitude driving, or desert conditions). Also the engine compartment temperature, greatly affect the compressor inlet temperature [138, Sec. 4.2]. Still, ambient gas temperature is sometimes used in modeling, even though large differences exist [86].

The basis for the map corrections is dimensional analysis [160], and the correction equations relevant for turbos are presented e.g. in [101], [38] and [174]. The correction equations scale the turbine and compressor performance variables, based on the current inlet temperature and pressure. An experimental investigation of the correction quantities for the compressor is presented in Paper 3, and an investigation on compressor inlet gas properties is presented in [18]. The inlet conditions for the compressor for an engine installation, for example, is affected by both a pressure drop due to the air filter and heat transfer in the pipes increasing the air temperature from ambient, see e.g. [85, p.38] and [147].

There are standards describing the procedures involved in measuring a turbo map, see e.g. [133], [134], [8] and [28]. The definition of when surge occurs, which gives the smallest mass flow point for a corrected compressor speed, have been discussed in a number of works, see e.g. [59] and [5]. In [109], detection of surge precursors is experimentally evaluated using pressure and temperature sensors at the compressor inlet and outlet. A summary of different turbo test facilities is presented in [59]. Methodology to measure turbo performance on an engine in a test stand is the topic of Paper 2.

2.5.1 Compressor map

There are four performance variables for the compressor map: corrected mass flow, pressure ratio, corrected shaft speed and adiabatic efficiency. The *corrected compressor mass flow* is given by

$$\bar{W} = W_c \frac{\sqrt{\frac{T_{01}}{T_{c,ref}}}}{\frac{p_{01}}{p_{c,ref}}} [\mathrm{kg/s}] \tag{2.3}$$

where $W_c[\mathrm{kg/s}]$ is the compressor mass flow, $T_{01}[\mathrm{K}]$ is the compressor inlet temperature, and $p_{01}[\mathrm{Pa}]$ is the compressor inlet pressure. The temperature $T_{c,ref}[\mathrm{K}]$ and the pressure $p_{c,ref}[\mathrm{Pa}]$ are the reference states. The reference states must be supplied with the compressor map, since these states are used to correct the performance variables. The *compressor pressure ratio* is given by

$$\Pi_c = \frac{p_{02}}{p_{01}} [-] \tag{2.4}$$

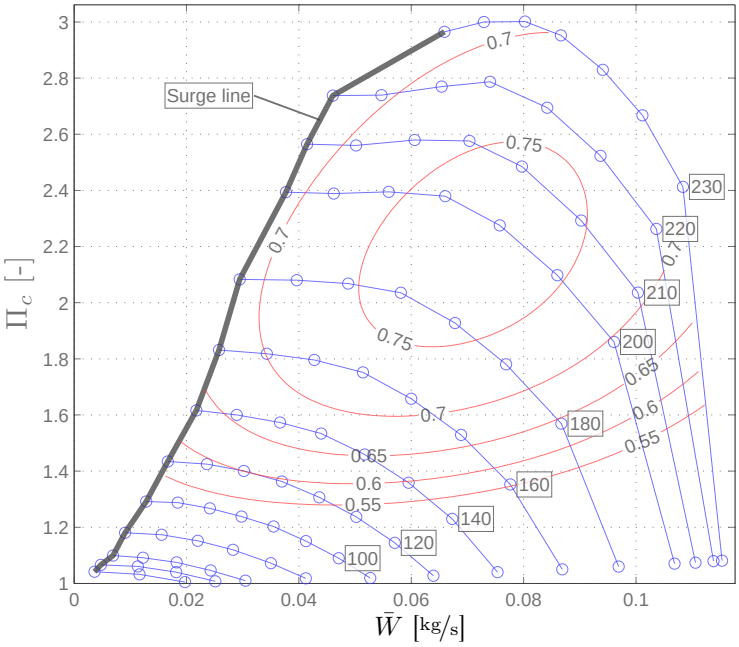

Figure 2.5: Example of a compressor map. The numbers in boxes indicate corrected shaft speeds $\bar{N}$ in krpm, i.e 180 means 180000rpm. Circles indicate measured points, and the contours represent the adiabatic efficiency. The surge line is also marked.

where p_{02}[Pa] is the compressor outlet pressure. The *corrected shaft speed* is defined as

$$\bar{N} = N_{\text{tc}} \frac{1}{\sqrt{\frac{T_{01}}{T_{c,ref}}}} [\text{rpm}] \tag{2.5}$$

where N_{tc} is the turbo shaft speed. The *adiabatic efficiency* of the compressor

$$\eta_c = \frac{\Pi_c^{\frac{\gamma_c - 1}{\gamma_c}} - 1}{\frac{T_{02}}{T_{01}} - 1} [-] \tag{2.6}$$

where γ_c [-] is the ratio of specific heats for air. The adiabatic efficiency describes how efficient the compression of the gas is, compared to an ideal adiabatic process. Or in other words, how much the pressure increases, compared to how much the temperature increases.

Points measured with equal $\bar{N}$ are connected in the compressor map, and are referred to as speed lines. A speed line consists of a number of measurements of Π_c and $\bar{W}$, and gives the characteristics of the compressor. Compressor efficiency η_c is also measured for each point, and contours of constant η_c are normally superimposed over the speed lines. The mass flows measured on each

speed line range from the surge line into the choke region. An example of a compressor map is shown in Fig. 2.5. The compressor models developed in Papers 1, 4 and 5 are given in corrected quantities.

2.5.2 Turbine map

As for the compressor map, there are four performance variables used in the turbine performance map: corrected mass flow, expansion ratio, corrected speed and adiabatic efficiency. It is further common to define two more variables for the turbine: turbine flow parameter and turbine speed parameter. The *corrected turbine mass flow* is given by

$$\bar{W}_t = W_t \frac{\sqrt{\frac{T_{03}}{T_{t,ref}}}}{\frac{p_{03}}{p_{t,ref}}} [\mathrm{kg/s}] \tag{2.7}$$

where $T_{t,ref}$[K] and $p_{t,ref}$[Pa] can be other standard states, than are used in the compressor map. The turbine mass flow W_t[kg/s], is the combustion products and thus normally the sum of fuel and air. The pressures p_{03}[Pa] and p_{04}[Pa] are the turbine inlet and outlet pressure, respectively, and T_{03}[K] and T_{04}[K] are the turbine inlet and outlet temperature, respectively. It is common to neglect the standard states in (2.7), and present turbine data using the *turbine flow parameter*, or TFP

$$\mathrm{TFP} = W_t \frac{\sqrt{T_{03}}}{p_{03}} [\mathrm{kg}\sqrt{\mathrm{K}}/\mathrm{s\,kPa}] \tag{2.8}$$

where p_{03} is usually given in [kPa], as indicated by the unit of (2.8). The *turbine pressure ratio* is here given by

$$\Pi_t = \frac{p_{03}}{p_{04}} [-] \tag{2.9}$$

Some authors prefer to have the pressure after the component divided by the pressure before as turbine pressure ratio as is the case for the compressor pressure ratio (2.4), this is however not chosen here to avoid having numbers of less than one. The *corrected turbine shaft speed* is given by

$$\bar{N}_t = N_{\mathrm{tc}} \frac{1}{\sqrt{\frac{T_{03}}{T_{t,ref}}}} [\mathrm{rpm}] \tag{2.10}$$

It is common to neglect $T_{t,ref}$ in (2.10) and define the *turbine speed parameter*, or TSP as

$$\mathrm{TSP} = N_{\mathrm{tc}} \frac{1}{\sqrt{T_{03}}} [\mathrm{rpm}/\mathrm{K}^{0.5}] \tag{2.11}$$

Since $p_{t,ref}$ and $T_{t,ref}$ are constants, neglecting them in equations (2.7) and (2.10) to give equations (2.8) and (2.11) respectively, gives only a scaling. The *adia-*

batic efficiency of the turbine is given by

$$\eta_t = \frac{1 - \frac{T_{03}}{T_{04}}}{1 - \left(\frac{p_{04}}{p_{03}}\right)^{\frac{\gamma_t - 1}{\gamma_t}}} [-] \tag{2.12}$$

where $\gamma_t[-]$ is the ratio of specific heats for the exhaust gas.

The high temperatures on the turbine side cause large heat fluxes. Measurement of T_{04} can have substantial systematic errors, due to the heat fluxes. An alternative efficiency definition for the turbine side is therefore commonly used, where no measurement of T_{04} is needed. The heat transfer effects are less pronounced on the compressor side, and the compressor power can be used to define an alternative turbine efficiency. The compressor power is given by

$$P_c = W_c \cdot c_{p,c} \left(T_{02} - T_{01}\right) [\mathrm{W}] \tag{2.13}$$

where $c_p[\mathrm{J/kg\,K}]$ is the specific heats at constant pressure. The alternative turbine efficiency definition includes the shaft friction, and is given by

$$\tilde{\eta}_t = \eta_t \cdot \eta_m = \frac{W_c c_{p,c} \left(T_{02} - T_{01}\right)}{W_t c_{p,t} T_{03} \left(1 - \left(\frac{1}{\Pi_t}\right)^{\frac{\gamma_t - 1}{\gamma_t}}\right)} \tag{2.14}$$

where the shaft friction is included in the mechanical efficiency η_m.

2.5.3 Measure maps

A turbo map is commonly measured in a gas stand. The gas stand has individual gas feeds to the compressor and turbine. The turbine feed gas is normally heated using e.g. a diesel burner. Different turbo operating points are measured after a thermal equilibrium is reached. Based on theory from dimensional analysis, corrected quantities are calculated from the mean values of the measured variables. These corrected quantities are then stored in a map. If care is taken to minimize external and internal heat transfer, a map referred to as adiabatic can be measured in a gas stand, this is however not common practice in industrial gas stand testing, see e.g. [145, p.11] and [11, p.1].

The compressor operating points are usually measured between what is referred to as the surge line, and up to what is referred to as the choke line or the stone wall. The turbine operating points are given by the compressor operation. Surge and choke are discussed below.

Normal gas stand turbine maps have a limited turbine flow range due to the restrictive flow ranges presented by the loading compressor. There exists different ways to wider the turbine flow range measured. The gas stand can be ran in closed-loop configuration, where the loading compressor inlet air density is increased using a feed back loop from the compressor discharge side. Another possibility is to replace the loading compressor with a dynamometer, or use a number of loading compressors. In [25] air injection nozzles are used on

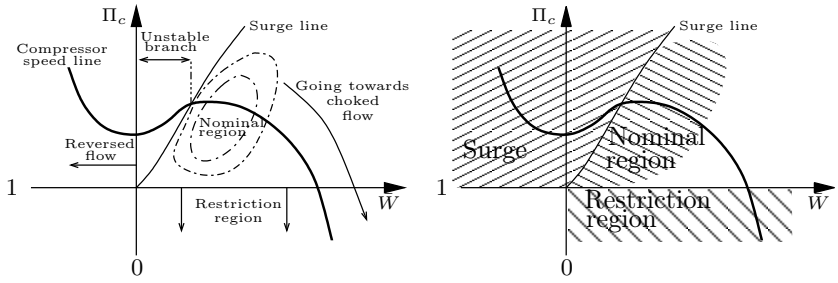

Figure 2.6: Schematic picture of the different compressor operating regions discussed in the text. The nominal region can be approximated with the efficiency contours shown. A decrease in mass flow to the left of the surge line can put the compressor in surge. The compressor is a restriction for $\Pi_c < 1$.

the compressor to increase the possible measured range in turbine flow. Measurements of permanent magnet eddy current dynamometer turbine maps are available in the literature, see e.g. [32] and [157, p.236].

A gas stand measured turbo map is a representation of the turbo performance on in the gas stand. The setup of the measurement equipment affects the performance, see e.g. [70, p.35], [88, p.323] and [13, p.123]. Further, the installation geometry and turbo operating conditions affects the performance, see e.g. [13, p.123], [138], or [107, p.227].

There also exist a spread in measured characteristics between turbo individuals of the same model, see [143] where a study focused on compressor characteristics resulting from introducing foreign objects into the impeller is presented. Measured characteristics of 40 turbos of the same model showed a relative difference between the measured pressure ratios of different chargers of approximately 1% at small flow, and approximately 2.5% for high flow. The corresponding relative difference for the measured efficiencies were approximately 1% at small flow and up to more than 5% at high flow. Further, the WG flow can affect turbine measured speed lines due to flow interaction in the outlet mixing chamber integrated in the turbine casing, see [25, p.100].

2.5.4 Compressor operation characteristics

In essence, the compressor map can be divided in three regions [170, p.33-34], exemplified in Fig. 2.6. The first is the normal operating region, which is stable. Left of this region, i.e. for smaller flows, is the unstable surge region going from the surge line and into negative flows. The surge line is commonly taken as the line connecting points with zero slope in the compressor characteristics,see e.g. [65, p.574]. For centrifugal compressors however, also positively sloped speed lines can be found, see e.g. [176, p.11]. The third region is associated with very high gas velocity, resulting in chocking in the limiting flow area of the machine. The compressor maps commonly supplied from the turbo manufacturers are usually focused on component operation at high efficiency, while the majority of engine operation is spent in regions that are not covered in

the standard maps, see [41]. Neither surge nor choke operation is covered in a standard map. The compressor models developed in Papers 1, 4 and 5 cover all three regions of compressor operation.

Surge and surge line

At least four different categories of surge, with respect to flow and pressure fluctuations can be distinguished, see e.g [34, p.1857] and [176, p.11]. The range goes from; mild surge, classic surge, modified surge, to deep surge. For mild surge, the annulus average mass flow oscillates, but remains in the forward direction at all times, see e.g. [51, p.322] and [35]. For deep surge, the order of magnitude of the negative flow rates is comparable to that of the positive flow rates, see e.g. [73, p.391]. Deep surge is said to occur for high speeds and pressure ratios, see [175, p.9].

Surge is said to occur for zero slope or slightly positive slope for vaneless diffusers and for slightly negative slopes with a vaned diffuser [129]. The positive slope itself is said to be related to the first stages of the instabilities associated with surge, see e.g. [149, p.66] and [57, p.1466]. In [177, p.258], it is stated that surge can also be induced for operating points on the linearly stable operating region of the characteristic, given an energetically large external trigger. There is also stated to be a line, referred to as the "Absolute stability boundary", from where and on surge will not occur independent on external triggers.

The simplest compressor system, made up by a control volume, a connecting pipe, a compressor and a throttling device, leads to a second-order differential equation for the system dynamics, see e.g. [69], [149, p.60] and [90]. The dynamic stability criterion resulting is due to inertia effects in the system and is referred to as the B-parameter, see e.g. [69, p.205]. The B-parameter is said to often be the governing criterion for compression systems, see [90]. Positively sloped points can be operated if the Greitzer B-parameter, see e.g. [69], is small enough (automotive sized compressors have $B \approx [0.5, 2]$, see [149, p.64]). Positively sloped speed lines are measured using active stabilization techniques in [177], where a loudspeaker is used as an actuator. Positively sloped points can further be measured if the discharge piping after the compressor is changed, see e.g. [51] and [58] where measurements of flow characteristics left of the surge line are presented. Stable positively sloped speed lines are measured down to close to zero flow, where the flow is said to exhibit some unsteadiness. Measurements of compressors driven with reversed flow using compressed air fed to the normal compressor outlet flange, are presented in e.g. [73] and [58]. A closely coupled valve is also used in [58] and [54], to measure compressor characteristics down to zero flow. Surge control using different actuators is investigated in [149, p.66], and it is found that the maximum slope that can be stabilized decreases as B increases, independent of actuator used.

The interaction between the compressor system components (impeller, diffuser, volute), leading up to instability is experimental analyzed and discussed in [179], where it is stated that surge is generally due to the interaction of the stalled and unstalled system components, and the tongue region is highlighted as important for system stability. The surge margin is said to improve with

a reduction of the number of diffuser vanes in [20, p.153]. The fluid dynamic circumstance leading to surge is, in [51, p.326], stated to be an inducer tip stall. The inducer tip flow reversal is most severe at the circumferential position corresponding to the volute tongue, for the particular compressor studied.

Given a system setup, surge can be seen down to very low speeds, see e.g. [73, p.392]. The surge line is further well defined and repeatable within 1% of maximum mass flow, see e.g. [51, p.324]. The position of the surge limit does not change in the compressor map with variation in the downstream volume, see [59, p.460].

In [88, p.325], an experimental study of how different compressor inlet geometries affects performance is conducted. Another investigation of surge lines for different system geometries are found in [54], where the surge occurrence dependency on installation conditions is measured and modeled. A comparison of surge line versus installation geometries is presented in [70, p.35]. The changing surge line positions for a two-stage system, compared to the individual units is highlighted in [173], where an increase in surge margin was found. The effect on the surge line from the test setup is also discussed in [106, p.598]. In [106, p.600], an increase in stable operation for unsteady flow conditions was presented. On-engine measurement of turbo surge limits are presented in [61, p.52], highlighting the importance of the compressor inlet piping. It is further shown that the surge line, in corrected variables, does not change with changing compressor inlet states (temperature and pressure), see [61, p.53]. It should be noted, though, that pulsations in the compressor inlet pressure also affect the surge margin, see [54].

Not only the surge behavior changes with size of downstream volumes, but also the power released during surge. Small control volume surge is assumed to be less harmful for the equipment in [68, p.850], and large volume surge makes extended surge measurements impossible, see [67, p.1342]. Surge further contributes to overall noise levels, see e.g. [35] and [166]. The operation on a compressor map point with a positive slope, is in [50] said to result in unstable running and generation of turbulence. This running is referred to as "marginal" or "soft" surge.

Surge operation and recirculation

When the compressor surges, some features of a surge cycle can be detected: flow reversal near constant pressure, an increasing mass flow at lower pressure, a rapid increasing mass flow back to a steady speed line point, and finally a an increase in pressure up to the point where the surge cycle starts again, see e.g. the surge measurements in [5, p.223]. The compressor operating points hence show a path dependent behavior during the stall and recovery processes, see [69, p.201]. Most of the surge cycle time is taken up by either emptying or filling the control volume downstream of the compressor, see [69, p.206-207]. The compressor moves quite rapidly between filling or emptying, and in addition, the filling period is generally longer due to the mass flow through the downstream throttle. At the end of the blowdown phase, the compressor reingests the residual hot gas present in the inlet, and this varying inlet gas

temperature and thus density contributes to a lag in the reverse to forward transition, see [51, p.325-326].

The surge frequencies are set by the overall systems dynamics and are, compared to rotating stall, not proportional to compressor speed. Changes in surge frequency with speed can be attributed to variations in e.g. the shape of the compressor characteristics, see [69, p.206-207] and [59, p.460].

Another phenomenon, closely related to surge, is rotating stall, which is a flow regime where stall cells propagate around the compressor circumference at speeds usually between twenty and seventy percent of the compressor speed [69, p.198]. In these stalled cells, negligible mass flow is at hand, and locally reversed flow can also be found. Rotating stall is though believed to have little effect on compressor performance, see e.g. [34, p.1857] and [175, p.10]. It is also stated in [175, p.10] that surge goes into rotating stall for a progressively reduced plenum size. In [120, p.106] it is stated that rotating stall occurs prior to surge initiation during turbo acceleration, and rotating stall is said to be observed prior to and following both mild and deep surge.

A connection between surge and recirculation, is presented in e.g. [5] and [106, p.598-600], where measurement of the gas temperature close to the compressor inlet is proposed as an indication of surge. Recirculation of air through the compressor system causes a drop in compressor efficiency for operation near the surge line [7]. The recirculation is due to the large pressure gradients existing in the compressor, and the clearances needed between compressor impeller wheel and volute. The recirculation mass flow thus follows the compressor shroud. In [70, p.26-27] both the temperature of and the amount of mass flow that recirculates are considered to be a functions of Π_c, independent on compressor speed. An increase in compressor inlet temperature with a decrease in W_c is there explained by the relative increase in recirculated mass flow, when the fresh air mass flow is reduced. Further, since the recirculation mass flow follows the shroud, a radial temperature gradient exists, which is said to be validated using measurements in [70, p.26-27]. The temperature increase due to backflow is measured in [5, p.226], and stated to be higher at the outer diameter of the inducer. Measurement of axial temperature distributions show larger temperature increases closer to the inducer. Measurement of the temperature increase when compressor operation approaches the surge line is presented in [61, p.51], where a high measured compressor inlet temperature is explained by the close proximity of the measurement probe, to the inducer. When surge is encountered, the temperature is said to suddenly increase up to the compressor outlet value. The recirculation is partly used to explain heat transfer modeling in [26, p.794], and in [27, p.245] it is stated that at low flows, some of the flow absorbs work but simply recirculates in the compressor inlet. A more consistent reverse flow is experimentally detected for smaller flows, causing an increase in inlet temperature in [106, p.598-600].

In e.g. [74, p.75], diffuser back-flow is said to occur in diffuser regions with high pressure and low velocity. Both fully and partly reversed flow is found at different instances and locations in the diffuser. Large radial pressure gradients are found at regions with fully reversed flow. The back flow is found to be able to go from the diffuser back to the compressor inlet region. It is in [74, p.79]

further stated that reversed flow on the suction side of the impeller vanes, due to the pressure gradients within the impeller, can exist even for increasing mass flow. In [180], the recirculation loss is said to dominate the disc friction loss under off-design operation. Thus the predicted efficiency curves are strongly influenced by the recirculation loss. Further, this loss is said to result from flow distortions at the impeller discharge section. When the flow is distorted enough, the flow separates close to the shroud and locally moves radially inwards and is again injected into the impeller flow.

Choke and restriction operation

The choke and restriction operating region is discussed in some papers, see e.g. [145], [79] and [49, p.40]. In [27] the operating characteristics for this region are estimated from normal compressor maps. The importance of this region for automotive applications are highlighted and exemplified, e.g. during tip-in or take-off or for unmatched operation of a two stage system. The operation in choke is further stated to be multi-valued in pressure ratio for a given flow. The restriction operation potential of the compressor was used in [116], where the compressor was used as a cold air turbine.

2.5.5 Turbine map characteristics

Compared to the axial flow turbine, the turbine map is noticeable wider due to the centrifugal field created by the rotor, see e.g. [170, p.34-35]. Compared to the compressor, the turbine map is still narrow in mass flow versus pressure ratio diagrams, and the efficiency map of a turbine is then plotted against the blade speed ratio. The blade speed ratio BSR relates the wheel tip speed of the turbine to the velocity equivalent of an isentropic enthalpy drop across the turbine stage, see e.g. [170, p.34-35, 152], as

$$\mathrm{BSR} = \frac{d_{t1}}{2} \frac{\omega_{tc}}{\sqrt{2c_{p,t}T_{03}\left(1 - \left(\frac{1}{\Pi_t}\right)^{\frac{\gamma_t - 1}{\gamma_t}}\right)}} \tag{2.15}$$

where d_{t1} is the outer diameter of the turbine wheel, $c_{p,t}$ and γ_t are gas constants.

Windmilling and turbine centrifugal pressure field

Windmilling refers to when the turbine acts as a bad centrifugal compressor and pumps in the "wrong" direction, due to the centrifugal pressure field created by the rotation of the turbine wheel, see e.g. [170, p.165-166, 185] and [172, p.150]. A certain turbine inlet pressure is required for the turbine flow to be in the correct direction already at low speeds, and this pressure increases with increased speeds since the centrifugal pressure field will oppose normal gas motion, see [170, p.185].

The centrifugal pressure field affects the full turbine flow range, and a greater turbine inlet pressure is required for a higher speed, given a mass flow [170,

p.185], however reversed turbine flow is usually not encountered, see [12, p.2], and is commonly neglected, see e.g [12, p.4] and [57, p.1467]. However the effect from the centrifugal force can be seen in data and used in models, see e.g. [145, p.78] and [112, p.13]. In [140, p.3739] the effect from the centrifugal forces are modeled using a changing effective equivalent nozzle area for the flow.

Unsteady turbine flow

The variation in turbine mass flow during an engine cycle is great, and the turbine can move from choked flow conditions to zero flow and back again, see [170, p.180] and [123, p.373]. Also negative flow parts can be found, see [178, p.198]. The complex pulse shapes resulting from engine operation, are primarily determined by the engine load, and the engine speed gives the frequency, see [108]. Instantaneous turbine torque is a function of the fluid state within the rotor passages and not at the turbine inlet, see [87, p.133], and to correctly estimate instantaneous turbine torque, care should be taken to account for possible mass/momentum accumulation inside the impeller channel, see [104].

The turbine efficiency η_t is generally lower if the turbine is operating under unsteady flow conditions, compared to the efficiency obtained in steady flow, see [170, p.165]. However some authors present the contrary, see e.g. [25, p.104]. A 10% loss in η_t for unsteady operation is presented in [81], and a 30% loss is stated in [85, p.43], and the losses are said to decrease with increasing pulse frequency, see [81].

Commonly a constant turbine outlet pressure p_{04} is assumed, though measurements show the contrary, see [12, p.9], and for a more thorough analysis also the p_{04} variations should be accounted for, see e.g. [24, p.557], [178, p.196,201] and [87, p.136]. However, in e.g [25, p.103] no appreciable p_{04} fluctuations are observed. Also the turbine inlet temperature T_{03} is sometime assumed to be constant, see e.g. [1, p.178], while other model T_{03} from the measured temperature signal and pressure, see e.g [12] and [53], as ${}^{T_3}/_{T} = \left({}^{p_3}/_{p}\right)^{({}^{\gamma_t - 1}/_{\gamma_t})}$, where T and p are the measured values for T_{03} and p_{03} respectively.

Pulsating flow through a twin entry turbine is studied in [32], where a quasi-steady behavior of the turbine stage in presence of pulsations typical of internal combustion engines is said to be insufficient. An extra volume is placed upstream of the turbine to model the effect of pulsations, but the rotor passages themselves are treated quasi-stationary with good results, see [32, p.2]. Measurements of unequal flow, as well as pulsating flows with different frequencies and phasing from a double entry turbine mounted in an eddy current dynamometer is presented in [30]. It is stated, that it is not immediately clear that a pulse event time an order of magnitude larger than the rotation of the wheel, will validate a quasi-steady assumption, see [30, p.5]. A significant overprediction of turbine efficiency is said to result, if the average velocity ratio and speed is compared to the steady-state equivalent, see [30, p.8], but a qualitatively sense of the expected performance will at least result. A further departure from quasi-steady operation was noted with an increase in pulse frequency in [30, p.10], while the contrary is presented in [87, p.136].

Measurement of circumferential pressure in the turbine volute is said to show

that the wave propagation speed is closer to the speed of sound, than to the bulk flow velocity, see [87, p.136]. It is further stated that at low frequency pressure wave propagation, the resulting wave shape is dominated by the effect of bulk mass transport, due to the very fast wave propagation compared to the pulse cycle time, see [32, p.3].

The static pressure development from the turbine inlet measuring plane to the rotor inlet is measured in [87, p.133], where it is shown that the pulse propagation is given by the appropriate sonic travel time. Exhaust pressure pulsations are estimated using N_{tc} measurements in [105], where it is also stated that the phasing of the exhaust pressure signal was clearly advanced compared to the turbo speed signal. The assumption of constant Tq_c is also questioned, and when using a high pressure EGR connection, the pulsating part of Tq_c is expected to increase, see [105, p.1190].

2.6 Model based control and mean value engine modeling

The use of mathematical models in an automotive control system is gaining increased interest from the industry. This increased interest comes from the complex engine concepts used, where additional actuators and degrees of freedom are added to the systems.

Complex boosting systems in series and parallel configurations are discussed in the literature. Series sequential control strategies are found in e.g [182], [29], [55], [118], and [63]. A parallel sequential turbo system for a heavy duty engine is presented in [16], where a larger turbo is used for the low speed operation and transient response. This larger unit is however smaller than the comparable single stage turbo unit, and is therefore improving performance. Also a smaller unit is engaged at higher engine speeds. An experimental study on a parallel system with unequal sized turbos is presented in [182]. A system with three turbos capable of both series and parallel operation is presented in [39]. Also turbo compounding, where the turbine torque is transfered directly to the crankshaft of the engine, or e-boost concepts, where an electric machine is connected to the turbo shaft are studied, see e.g. [45].

Model based control is proposed as a way of handling the increased complexity. The models are used for a number of things. Simulation environments can be constructed around the models to aid for example in controller design, in concept evaluations, or in the parametrization process of other controller structures, see e.g. [167], [164] and Paper 1. Observers can be built around the models to estimate non measured states of the system, see e.g. [15] and [6]. A direct use of an inverse model can be made, to handle a nonlinearity of a system, see e.g. [162], and [165]. Model based diagnosis is another example of an important field for control oriented models, see e.g. [119]. The model based control approach have been studied for different automotive control applications, for example in [67], [3], and [121].

Mean Value Engine Modeling (MVEM), see e.g. [75], [83], [76], [48], [43], [85] and [21], is a modeling framework used in the automotive society. MVEM

usually means that the model is based on average values of the engine cycle, i.e. in-cylinder processes such as valve opening and closing are averaged out. This simplification means that vehicle test cycles, consisting of many minutes of driving, can be simulated on a normal PC, with short calculation times.

In the full system modeling presented in Papers 1 and 4, the turbo model is implemented as part of an MVEM framework.

2.7 Model families

A model is here classified dependent on the complexity and computational burden of the model.

Gas motion can be modeled in 3D, e.g. solving the Navier-Stokes equations of gas motion numerically. Such modeling needs accurate geometric information of the system, see e.g. the complex impeller geometries of Fig. 3.1. The boundary conditions of the model are further important, i.e. how the gas enters and leaves the modeled component. Due to the complexity and the computational effort [11, p.1], these models are most often only used to model components of the engine, see e.g. [181], [71], and [74]. In [103], the 3D models are said to be worthwhile for detailed optimization of turbine aerodynamics, but else too demanding both in computational power and calibration effort. The solutions obtained, give valuable information of for example the gas motion, that can be used also for less complex model families. Also the reverse is true, see [27]; good models from less complex model structures can be used on a component level for a 3D simulation.

Another level of detail that is frequently used, is the 1D model family. They model the gas flow along pipes and account for properties in this dimension. 1D models of compressors are however rarely found. The computational cost is reduced, compared to 3D models, and large parts of an engine system can be simulated with reasonably short simulation times.

The last model class is given by the 0D models. The 0D models can be further divided in physical models and black or gray box models. The physical turbo models typically starts with an ideal component, and then subtracts different losses to give the component performance. The modeling effort is then concentrated to models for different losses. The black and gray box turbo models utilizes that turbo performance is conveniently given by the performance maps, and use curve fitting to the map variables. The modeling effort is then concentrated to developing mathematical functions that can be curve fitted to the data, and that gives good description of the component performance.

The following sections will present 0D models for the turbine and friction, while physical and black or gray box modeling of the compressor is presented in Chapter 3.

2.8 0D turbine modeling

This section presents a brief summary of turbine models available in the literature. To agree with the model complexity of the compressor models developed

in this thesis, only 0D models will be presented here. However physical models in 1D or 3D also exist, see e.g. [154]. A further division of the modeling effort is commonly chosen, where turbine mass flow and turbine efficiency are separately modeled. This division is also chosen here, and the modeling of the mass flow dimension of the turbine map is presented first, followed by turbine efficiency models.

2.8.1 Turbine mass flow modeling

A simple and well used model for turbine mass flow is based on the so-called single line characteristics, where a mean curve is drawn through the complete turbine map flow data, ignoring any variation with speed, see e.g. [9, p.162]. Compared to an axial turbine, neglecting speed can introduce substantial errors since the radial flow turbine shows a significantly wider flow map due to the centrifugal fields, see e.g. [79, p.72]. Many turbine mass flow models rely on the use of a nozzle equation, see e.g. [169, p.127], [170, p.541] and [78, App.C2], as

$$\dot{m}_t = \begin{cases} \frac{C_d A p_{03}}{\sqrt{RT_{03}}} \cdot \Pi_t^{-\frac{1}{\gamma_t}} \sqrt{\frac{2\gamma_t}{\gamma_t - 1}\left(1 - \Pi_t^{\frac{1-\gamma_t}{\gamma_t}}\right)} & \Pi_t < \Pi_{t,crit} \\ \frac{C_d A p_{03}}{\sqrt{RT_{03}}} \cdot \sqrt{\frac{2\gamma_t}{\gamma_t + 1}^{\frac{\gamma_t+1}{\gamma_t-1}}} & \text{else} \end{cases} \tag{2.16}$$

for the turbine case using $\Pi_t = {}^{p_{03}}/_{p_{04}}$. The critical pressure ratio $\Pi_{t,crit}$, determining whether the flow is choked (sonic) or not (subsonic), is given by $\Pi_{t,crit} = \left({}^{2}/_{(\gamma_t+1)}\right)^{\gamma_t/(1-\gamma_t)}$. For $\gamma_t = 1.3$ and $\gamma_t = 1.4$ this gives a $\Pi_{t,crit} = 1.832$ and 1.893, respectively. However, the turbine does not choke completely even for this pressure ratio, and a better model is said to be obtained using two orifices in series, see e.g. [170, p.546] and [140, p.3730]. The same line of thought is followed in [79, p.70], where also the pressure losses due to fluid friction is accounted for resulting in a maximum pressure ratio capability of roughly 4 being expected for a single-stage turbine. It is further noted in e.g. [152, p.3], that the nozzle model is valid for steady flow states and boundary geometry being sufficiently smooth functions in a spatial variable. It is also important to note the the effective throat area is not made up by the only the geometrical layout but also the gas angles, in order to represent accurately the fluid-dynamic behavior of the turbine see [170, p.187] and [140, p.3730].

A model of different actuated turbines are found in [140]. The model is based on estimation of reaction degree of the turbine, and one nozzle model is parametrized for the stator and one for the rotor, see [140, p.3732]. A degree of reaction of 0.5, meaning that the same pressure drop occurs across the rotor as across the stator, is said to be the case for turbines without guide vanes, and radially vaned rotors, see [140, p.3731]. The degree of reaction assumption of 0.5 is, however, said to not necessarily be true for variable geometry turbines, see [140, p.3732].

Unsteady turbine flow performance is commonly accounted for using different scaling factors, adjusting the steady performance curves, see e.g. [12, p.1], [170, p.152 or p.520-521], and [25, p.97]. The scaling factors can be constant [19,

p.26], or vary with other parameters. The pressure pulse shape at the turbine inlet is commonly characterized by its frequency and amplitude [1, p.178]. The turbine mass flow scaling factor is stated to not be affected by heat transfer, see [2]. In [24, p.559] for a VGT, the only decisive trend with the pulse characteristics (amplitude and frequency) is said to be found for the mass flow factor, which shows a generally reducing trend with increased pulse amplitude. To handle VGT turbines, a turbine flow model is commonly adapted to each discrete VGT position measured, and interpolation between these models is then used. The variation between different VGT positions is however not linear, see e.g. [158, p.147].

In [145], a comparison of turbine performance for different turbine inlet temperatures can be found. The investigation shows that the turbine flow lines, measured for different turbine inlet temperatures differ rather much. The lower turbine inlet temperature, the lower reduced turbine flow given a turbine pressure ratio, see e.g. [145, p.78].

Examples of 0D turbine flow models In [83, p.4], the turbine flow characteristic was described using the concept of an equivalent turbine area $A_{t,eq}$, defined as that area which gives the correct turbine flow, when the turbine inlet temperature and overall pressure ratio are used in the isentropic flow equation. The equivalent turbine area is modeled as using an affine function in Π_t, where the affine coefficients in turn given by affine function in TSP. A slight variation to this model structure is proposed for a VGT in [112, p.11-13], where second order polynomials are used for the coefficients of the affine equivalent turbine area model, and the zero pressure ratio is taken into account using a quadratic function in VGT position. In [155, p.124] a two flow region turbine pressure ratio model is proposed, that uses a second order polynomial in $^{\mathrm{TFP}}/_{A_{t,eq}}$ for the lower flows, and an affine model for higher flows. A model where Π_t is given only as a second order polynomial in actual flow W_t is presented in [48, p.135]. A model in corrected turbine flow $\bar{W}_t$ is also presented in [48, p.136] as

$$\bar{W}_t = c_1 \sqrt{\max\left[0, 1 - \Pi_t^{-c_2}\right]} \tag{2.17}$$

This model is also used in [6, p.116], [44, p.534]. A closely related model is presented for a VGT in [168, p.972]. A model giving actual turbine flow W_t as a function of Π_t, is presented in [135], as $W_t = C_1 \left(1 - e^{-C_2 \Pi_t^{C_3}}\right)$ where C_1, C_2, C_3 are second order polynomials in VGT position. The model structure is also used in [62, p.1412]. In [22] a variation to (2.16), stated to be valid assuming the flow to be adiabatic and irreversible, is introduced as a model for actual flow of a VGT. Another VGT flow model is presented in [122, p.385], where the turbine outlet pressure and temperature are used as input to the model. A variation to the effective area turbine flow model is presented in [41], where again an exponential function is utilized

2.8.2 Turbine efficiency modeling

General thoughts on turbine efficiency models are found in [170] and [9], where it is stated that if turbine efficiency is plotted against blade speed ratio BSR, the effiency lines collapse into a narrow band at least for the lower speeds and pressure ratios. At higher speeds, a decreasing efficiency is expected, for a nozzleless turbine, due to the high gas velocities that these speeds imply. Further, it is stated that for turbines tested on dynamometers, the efficiency curves extend to both higher and lower values of BSR in a regular manner [9, p.163-164]. The turbine isentropic efficiency is not easy to measure and results can vary greatly dependent on test conditions, where e.g. turbine efficiency measured for varying turbine inlet temperature will be different due to the change in heat transfer [170, p.165].

Studying the connection between BSR and η_t, the following can be seen as a rough guideline, see e.g. [170, p.165-166], [9, p.165], and [47, p.160]. The efficiency must, from physical consideration, be zero at two points given a speed; for BSR $= 0$, and for a BSR $\in [1.1, 1.2(1.3)]$. The latter point is given by the, with speed, varying centrifugal pressure field, giving rise to a varying pressure ratio at zero flow, see Section 2.5.5. Beyond this point, the turbine will act as a compressor. A speed dependent maximum efficiency point occurs between these two outer points, at a BSR $\in [0.6, 0.7]$. For turbines where the maximum efficiency varies significantly with speed, separate curves for different speed ranges can be defined. These three points can then be connected using a cubic curve, so that the a rather steep drop in efficiency occurs for BSR > 0.8.

Examples of 0D turbine efficiency models In [83, p.3] the turbine efficiency is described as essentially a function of BSR, and the efficiency is modeled using a third order polynomial in BSR, where the coefficients C_i of the polynomial are in turn parametrized $C_i = {}^{(c_{i,1}+c_{i,2}N_t)}/_{(c_{i,3}-N_t)}$ with $i \in \{0, 1, 2, 3\}$, and N_t is described as turbine rotational speed. End points for low and high BSR were added, in [83], in the fitting procedure to ensure a sound extrapolation. The same η_t-model structure is presented in [112, p.13], where $C_0 = 0$ is used. In [155] a model for η_t is proposed as $\eta_t = c_1 C_2 \left(1 - (1 - {}^{\text{BSR}}/_{0.61})^2\right)$ where c_1 is the peak efficiency for any operating point, and $C_2 = \left(c_2 \Pi_t^2 + c_3 \Pi_t + c_4\right)$. In [72] the following model is given

$$\eta_t = C_1 \left(2\frac{\text{BSR}}{C_2} - \left[\frac{\text{BSR}}{C_2}\right]^2 \right) \tag{2.18}$$

For a turbine with variable nozzle area, C_2 is said to be a function of the VGT position, with only a minor effect on C_1. The same model is used in e.g. [6, p.118] and [44, p.533]. In [126, p.5] the same model structure is used for a fixed geometry turbine, and for a VGT also C_1 is a proposed to be a function of the VGT position. In [112, p.13] a model is proposed where η_t is given as a second order polynomial in BSR, with the coefficients of the polynomial in turn given as first order polynomials in N_{tc}. In [48, p.136] the following η_t-model is proposed as $\eta_t = c_1\sqrt{\Pi_t - 1} + c_2\sqrt[4]{\Pi_t - 1} + c_3$. A third order polynomial in BSR is

proposed as a η_c-model for a VGT in [122, p.386], where the polynomial coefficients are parametrized as second order polynomials in N_{tc} and VGT control signal u_{VGT} as $C_i = c_{i1} + c_{i2}N_{\text{tc}} + c_{i3}N_{\text{tc}}^2 + c_{i4}u_{\text{VGT}} + c_{i5}u_{\text{VGT}}^2 + c_{i6}u_{\text{VGT}}N_{\text{tc}}$ for $i \in \{0, 1, 2, 3\}$.

2.9 0D friction modeling

In [9, p.117] Petroff's equation is used to estimate journal bearing frictional torque as

$$Tq_{fric} = \frac{\pi}{4}\frac{\mu L D^3}{\epsilon_r}\omega_{tc} \tag{2.19}$$

where μ is the oil viscosity, ω is the rotational speed, L and D are the bearing length and diameter, and ϵ_r is the fluid film thickness. The friction power loss in a plain, double-sided thrust bearing is in [9, p.124], modeled using Petroff's equation. Since $P = Tq \cdot \omega$, the corresponding friction torque is given by

$$P_{fric}/\omega_{tc} = Tq_{fric} = \frac{\pi\mu\left(r_o^4 - r_i^4\right)}{\epsilon_z}\omega_{tc} \tag{2.20}$$

where r_i and r_o are the inner and outer radii of the thrust bearing, and ϵ_z is the axial clearance. The journal bearing friction power is in [114] modeled, assuming viscous friction, as $P_f = (2\pi n_{tc})^2 k_f = k_f \omega_{tc}^2$ and hence $Tq_{fric} = k_f \omega_{tc}$, where $k_f = 3.23 \cdot 10^{-6}\,\text{kg}\,\text{m}^2/\text{s}$ for a GT1749MV turbo.

In [172, p.78] it is stated that a detailed friction model should divide the friction loss at least into thrust bearing friction and radial bearing friction. In [137, p.194] it is concluded that a friction model that only depends on charger speed is insufficient, and that a more detailed modeled should include axial force, oil temperature and oil pressure. It is further concluded that the friction power polynomials delivered by the turbo manufacturer of the form $Tq_{fric} = a \cdot N_{\text{tc}} + b$ with constant a and b does not fit the measured friction, and shows up to 70% error compared to the experiments. Therefore, an improved model is proposed as $Tq_{fric} = a \cdot N_{\text{tc}}^b + c$, in [137, p.195]. A constant friction or an affine model in N_{tc} is said to be adequate in [36]. A linear Tq_{fric}-model in ω_{tc} is used in [6, p.122], where the constant is tuned manually. The friction losses are however often neglected, see e.g. [72, p.63] and [41], but the addition of a friction torque can be beneficial in some situations, see [72, p.64].

2.10 Turbine and friction models used in Papers 1 and 4

Both a turbine and a friction model are needed for the full engine simulations presented in Papers 1 and 4. While the compressor modeling is devoted the entire Chapter 3, the turbine and friction models used in these papers are briefly presented here.

The gas properties are first assumed to be constant. The turbine model is divided in a flow and an efficiency submodel. During the full system simulations, the turbo model was implemented as part of an MVEM. This means that unsteady flow due to cylinder pulsations are neglected. Further, the full system simulations presented in Papers 1 and 4 are mainly studies of surge, where usually a fully opened WG is commanded once surge is encountered. Hence, oscillations in turbine inlet states will decrease substantially. However, just prior to surge initialization the system is commonly operated with large oscillations in turbine inlet states. Turbine unsteady performance was then accounted for using scaling factors. The modeling further assumed that any heat transfer affecting the performance was already accounted for in the efficiency of the measured maps, e.g. using adiabatic map measurement procedures.

The turbine flow model is formulated in the corrected variables of the turbine map. Hence, the model utilizes dimensional analysis derived corrections to calculate turbine performance for variations in turbine inlet conditions. The model from [48] given by (2.17) is used, i.e.

$$\bar{W}_{t,mod} = c_1 \sqrt{\max\left[0, 1 - \Pi_t^{-c_2}\right]} \tag{2.21}$$

where the parameters c_1 and c_2 are estimated using nonlinear least squares. The model provides good fit to the available data for the turbines tested. The model hence neglects windmilling. Given a turbine pressure ratio Π_t this model is used to calculate $\bar{W}_{t,mod}$. Using the reference states $T_{t,ref}$ and $p_{t,ref}$, a turbine inlet temperature T_{03} and turbine inlet pressure p_{03}, a modeled actual turbine mass flow $W_{t,mod}$ is then calculated using (2.7).

The efficiency model makes use of the model from [72] given by (2.18) with a lower saturation on efficiency as

$$\eta_{t,mod} = \max\left[\eta_{t,\text{lower sat.}},\ C_1\left(2\frac{\text{BSR}}{C_2} - \left[\frac{\text{BSR}}{C_2}\right]^2\right)\right] \tag{2.22}$$

The model is parametrized to the manufacturer maps using nonlinear least squares. It should be noted that the manufacturer maps commonly calculates η_t using (2.14), and friction is hence included in this efficiency. Still, a separate friction model will be added, see below. Given model parameters, and BSR (from (2.15)), a modeled efficiency can be calculated. Using the modeled efficiency, Π_t and T_{03}, the turbine outlet temperature $T_{04,mod}$ is modeled using (2.12). The modeled turbine power is then calculated using (2.13) with changed subscripts as

$$P_{t,mod} = W_{t,mod} \cdot c_{p,t}\left(T_{03} - T_{04,mod}\right) \tag{2.23}$$

and the modeled turbine torque, Tq_t of (2.1), is given by

$$Tq_{t,mod} = \frac{P_{t,mod}}{\omega_{tc}} \tag{2.24}$$

The friction torque model $Tq_{fric,mod}$ is linear in ω_{tc}, and given by

$$Tq_{fric,mod} = c \cdot \omega_{tc} \tag{2.25}$$

where c is a constant. This model hence corresponds to the model in e.g. [114]. The constant c collects the geometric and oil properties of either (2.19) or (2.20). Friction is already accounted for in the η_t-model, but a separate friction model is still used since this increased the stability of the simulations.

3

Compressor modeling

This chapter presents an overview of compressor modeling efforts found in the literature, that have been the inspiration and motivation for the compressor model that is developed in this thesis.

Compressor operation can naturally be divided into three different regions: nominal operation, choke or a restriction like operation, and surge. A sketch of the different regions is presented in Fig. 2.6, and the modeling overview presented here is divided into these three parts. Surge, restriction and choke are discussed first. This is followed by modeling for mainly the normal operating region. The physical modeling approach is presented first. Even though the models developed in this thesis are not of the physical model family, a good overview of the modeling challenge and the phenomena that affects compressor performance, is gained from briefly presenting this model family. An overview of black and gray box compressor modeling is then given, and a number of models are exemplified, demonstrating the wide range of available models. An overview to the compressor models developed in this thesis are presented in the final section.

3.1 Compressor surge modeling

To model surge many authors follow the Moore-Greitzer approach, see e.g. [69] and [111]. A compressor mass flow state is introduced where, due to the gas inertia, the compressor mass flow deviates from stationary performance curves for a transient, see e.g. [58]. The version of the Moore-Greitzer state used in this thesis is

$$\frac{dW_c}{dt} = \frac{\pi d_c^2}{4L_c}\left(\hat{p} - p_{02}\right) \tag{3.1}$$

where $\hat{p} = \hat{\Pi} \cdot p_{01}$ is the compressor pressure build up during stationary operation, d_c is the compressor diameter, and L_c is the duct length. p_{01} and p_{02} are set by the system, while $\hat{p}$ (and $\hat{\Pi}$) is a measure of the pressure the compressor builds given an operating point. Using the model (3.1), it is hence only for stationary operation that $p_{02} = \hat{p}$.

Good summaries of surge modeling efforts are found in [34] and [176]. Compressor operation with negative flow is modeled as a parabola in [73, p.392] and [129]. A model like $\Psi_c = c_n W_c^2 + \Psi_{c,0}(\omega_{tc})$ was proposed for negative flows in [65, p.572], [67, p.1344] and [68, p.853], regarding the compressor as a throttling device with a positive pressure bias. The model is parametrized to give a negative slope of the compressor characteristic for negative flow. A second order polynomial was used as a negative flow model in [161]. In [175, p.9] it is stated that the compressor works on the steady-state back flow characteristic during the emptying phase of a surge cycle, where the steady-state back flow characteristic is defined as the resistance which the rotating blades offer to flow in the reversed direction. This characteristic is further thought to be of roughly parabolic shape. The negative flow region is modeled as $\Pi_c = \Pi_{c0} + cW_c^2$ in [70, p.67]. The reverse flow region is considered to be modeled as an isothermal flow process in [58, p.822] and in [54]. In [127, p.235], a methodology to measure ceramic rotor components is presented, where the compressor wheel is supplied with compressed air from the normal compressor outlet, and the compressor is hence used as a turbine in the measurements.

The region between the surge line and zero flow is modeled as a cubic polynomial in [73, p.394], where it is further stated that the exact modeling of the unstable branch could not be verified experimentally, but that sample calculations show the influence from the speed line shape to not greatly affect the simulations, due to the comparatively small time spent in that flow region. The same conclusion is drawn in [129]. A third order polynomial was also used as flow model for this flow region in [161]. In [70, p.66] the following was proposed as a model for the flow region between zero and the surge line $\Pi_c = \Pi_{c0} + \Pi_{c,\beta}\left(3\left({}^{W_c}/_{W_{c,\alpha}}\right)^2 - 2\left({}^{W_c}/_{W_{c,\alpha}}\right)^3\right)$.

The compressor pressure ratio at zero flow Π_{c0} can be modeled using radial equilibrium theory for the compressor impeller blades as

$$\Pi_{c0} = \left(1 + \frac{\gamma_c - 1}{2\gamma_c R T_1}\omega_{tc}^2 \frac{d_{c2}^2 - d_c^2}{4}\right)^{\frac{\gamma_c}{\gamma_c - 1}} \tag{3.2}$$

assuming no losses in the compressor impeller, see e.g. [161], [129], [70, p.66], [67, p.1344] and [66]. In [22], the same model is referred to as the "vortex equation", and in [17, p.136] another closely related formulation is given. It can be recognized that zero pressure build up is closely related to the discussions in Section 2.5.5, where an increasing Π_t with speed is found for zero turbine flow.

In [58], measurements of Π_{c0} shows good agreement with (3.2), especially for low to medium speeds. In [35], a gain is added to the model (3.2). The extended model is said to give good agreement with experimental data for low to medium speeds, with a gain close to one. The discrepancies are however increasing for higher speeds. In [54], Π_{c0} is closely related to the surge trajectories in the

compressor map at nearly constant compressor speed, going from the maximum compressor pressure ratio, found close to the surge line, to the minimum pressure ratio found at zero flow.

Modeling of surge for a parallel sequential turbo system is presented e.g. in [159] and [163]. Extensions of 1D models to also incorporate surge is presented in e.g. [58] and [35]. However, the underlying surge model is commonly taken as a lumped parameter 0D model.

3.2 Restriction and choke modeling

Two modes of compressor operation with $\Pi_c < 1$ are proposed in [145, p.16]. If a driving compressor torque results, the compressor operation is said to be as an abnormal turbine. Otherwise, the compressor is said to work as a throttle. A cold air turbine efficiency for the compressor of 20% is assumed for the compressor restriction operation in [116, p.4-7], where further a typical nozzle discharge characteristic is said to be apparent. Compressor speed line extensions below a compressor pressure ratio of unity is presented in [79, p.73]. The restriction operation for a mismatched operation of a single turbo system, or in a two-stage compression system is recognized in [27, p.240]. The model proposed in [27, p.247] is extrapolated down in Π_c to where the impeller outlet temperature equals the inlet. From this point downwards the compressor is said to work as a rather poor turbine, with excessive kinetic energy at the outlet.

Choking is discussed and modeled in [170, p.133], where reference is made to an earlier version of [38]. Assuming all flow processes to be adiabatic and the fluid as a perfect gas, the inducer choke flow is modeled as

$$W_c = A_{eff}\rho_{01}a_{01}\left(\frac{2}{\gamma_c+1}\right)^{(\gamma_c+1)/2(\gamma_c-1)} \tag{3.3}$$

where A_{eff} is an effective flow area, ρ is density, a local speed of sound, and γ_c is a gas constant, see e.g. [170, p.133], [38, p.230], [65, p.574] and [156, p.655]. Further it is noted that A_{eff} is the flow area, made up of both the geometric area and the blockage, see e.g. [156, p.655] and [27]. Assuming an isentropic flow, choking in the impeller is modeled as

$$W_c = A_{eff}\rho_{01}a_{01}\left[\frac{2+(\gamma_c-1){U_c}^2/a_{01}^2}{\gamma_c+1}\right]^{(\gamma_c+1)/2(\gamma_c-1)} \tag{3.4}$$

where $U_c = {}^{d_c}/_2 \cdot \omega_{tc}$, see e.g [64, p.346] and [38, p.231]. The choking mass flow dependency on blade speed is explicitly shown, with a greater limiting mass flow found at higher speeds. A small variation to this model, where $\left({}^{d_c}/_{d_{c2}}\right)^2$ is added before U_c, is presented in [27]. The steep fall off in work input at very high flow on the high-speed characteristics, due to the choking of the flow in the impeller inlet, is discussed in [27, p.243], and used to determine the value of A_{eff}. It is stated that the calculated A_{eff} for each high-speed curve show a reasonable constant value, hence that A_{eff} is not strongly affected by the speed. The compressor density ratio associated with the choking was further

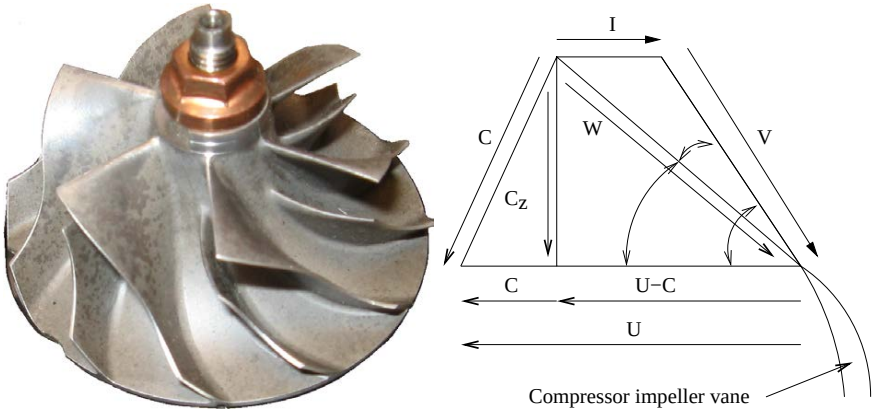

Figure 3.1: Picture of an impeller and the inducer velocity triangle. The Z-axis goes through the turbo shaft, W is the relative flow vector between the gas velocity vector C and the vane velocity vector U. The incidence loss in the inducer is connected to the velocity I. δ denotes the vane angle.

used to calculate the losses associated with choke [27, p.246]. The diffuser inlet conditions depend on the impeller properties. In e.g. [170, p.133] and [38, p.232] the following is proposed as a model for diffuser choking flow

$$W_c = A_{eff}\rho_{01}a_{01}\frac{1+(\gamma_c-1)\eta_{imp}\sigma\, {U_2^2}/{a_{01}^2}}{\left[1+(\gamma_c-1)\sigma\, {U_2^2}/{a_{01}^2}\right]^{1/2}}\left(\frac{2}{\gamma_c+1}\right)^{{(\gamma_c+1)}/{2(\gamma_c-1)}} \tag{3.5}$$

where σ is the slip, η_{imp} is the impeller efficiency, and $U_2 = {d_{c2}}/{2}\cdot\omega_{tc}$ is the impeller exducer tip speed.

3.3 Physical modeling

The physical compressor model family is based on modeling the different losses that affect the fluid flow through the compressor. These models often make use of the velocity triangles, which are exemplified for the impeller entry in Fig. 3.1. An ideal compression process is commonly assumed, and losses are modeled and subtracted from the ideal component performance. This section presents modeling thoughts from the physical compressor modeling family, and a summary of the major compressor stage losses and velocity triangles are given in any of the basic turbocharging references, see e.g. [170, p.128], [38, p.202] and [9, p.56]. Some examples of physical model implementations can be found in e.g. [64] and [117]. Its common in the analysis to assume that both the inlet and outlet angles of the flow are considered given by geometric characteristic of the blade shape, but this is not rigorously true, since the angles depend on the flow physics, see e.g. [60], [64] and [65]. The angles also vary with radius and axial location, see [60] and Fig. 3.1.

A gas element is followed through the compressor stage components, and the first losses occur since the gas has to comply with the vane geometry at

the impeller inlet. These losses are referred to as incidence losses, and are due to that the inducer relative velocity vector W does not agree with the vector parallel to the vane surface V, see Fig. 3.1. The incidence loss connected to the velocity I can be modeled in different ways. In [65] two methods are given. (I): the "NASA shock loss theory", which is based upon the destruction of the kinetic energy associated with the velocity I. (II): a constant pressure incidence model, where it is assumed that the flow just inside the blades has adapted to the blades via a constant pressure process.

The concept of slip σ is commonly used to model the guidance the fluid attracts from the impeller vanes, and is discussed and modeled in e.g. [101], [38] and [128]. Generally, the less guidance the gas attracts from the vanes the more slip. The more guidance, the more friction. Slip is commonly modeled using the Stanitz formula as $\sigma = {}^{S}/_{U} = 1 - {}^{2}/_{n_b}$, where S and U are fluid velocities, and n_b is the number of blades. Another model of slip is found in [82, p.190]. In [113, p.6], it is stated that the entire number of blades (both splitter and normal blades) should be considered, since there is no difference between these two vane types at the impeller outlet. In [27, p.242,245] it is stated that the slip factor might not be constant along a speed line, but that the slip factor is generally constant for a given flow coefficient. For high flows though, the slip factor may change.

The fluid friction losses due to the gas viscosity and motion through the compressor are modeled e.g. in [64], [67], and [174]. The losses due to fluid friction against the impeller and stationary components are described in e.g. [47, p.144]. More details of impeller friction losses can be found in [170, p.99-100]. It is further stated in [170, p.100] that at pressure ratios commonly found in automotive turbos, the diffusion and the blade loading losses are usually not the dominant losses, and that these losses can therefore conveniently be included in the surface friction loss coefficient.

Models of recirculation losses are presented e.g in [84] and [65]. The back flow losses, both along the shroud and across the blade tip from the pressure to the suction side of the vanes, is suggested to be modeled as a decrease in stage efficiency of $\Delta\eta_{bf} = 0.03$ in [47]. The back flow loss due to that the compressor reprocesses fluid, that is reinjected into the impeller due to the pressure gradients existing in the impeller tip region, is modeled using a constant flow loss $\Delta\eta_{bf}$ in [65]. From [84] the loss in efficiency due to clearance can be expressed as $\Delta\eta_{cl} \approx 0.3{}^{L_{\mathrm{cl}}}/_{\mathrm{b}_2}$, where L_{cl} is the tip axial clearance and b_2 is the impeller tip width. In [90], the impeller/diffusion interaction is captured by a recirculation loss bucket, and the leakage flow is modeled. In [74], losses due to the "tongue" are presented. The "tongue" is here part of the geometrical shape of the volute located where the downstream piping connects.

Incidence losses using a vaned diffuser are discussed in [60]. Experimental investigations of the gas motion in the diffuser is found e.g in [136]. The main cause of the diffusion process losses are said to be separation of boundary layers and fluid friction, see [38].

Models of the volute losses are described e.g. in [170]. In [65], the volute loss is said to be approximately $\Delta\eta_{vl} \in [0.02, 0.05]$, and likely higher for vaned diffusers. In [42, p.779] it is stated that the inlet ducts and volute loss typically

account for roughly $4-6$ points in efficiency decrement. In [84, p.1336], it is noted that the relative magnitude of clearance, backflow and volute losses decreases gradually as mass flow rate goes up, due the increase in incidence losses and friction losses at higher mass flow rates. Disc friction losses are modeled in [180]. Losses due to choking are modeled in [27].

3.4 Black and gray box compressor modeling

Black and gray box compressor models are curve fitting based approaches, that recognize that all performance variables are conveniently given by the speed lines and the efficiency contours of the map. The modeling effort is then to fit different curves to the map, or to a transformed map. The semi-physical gray box models usually transform the compressor map variables into the dimensionless head parameter Ψ_c, the dimensionless mass flow coefficient Φ_c, and the inlet Mach number M_c as

$$\Psi_c = \frac{c_{p,c} T_{01} \left[\Pi_c^{(\gamma-1)/\gamma} - 1 \right]}{0.5 U_c^2} \tag{3.6}$$

$$\Phi_c = \frac{W_c}{\rho_{01} \cdot \pi/4 \cdot d_c^2 \cdot U_c} \tag{3.7}$$

$$M_c = \frac{U_c}{\sqrt{\gamma_c R T_{01}}} \tag{3.8}$$

Connections between Ψ_c, Φ_c and M_c are then parametrized and used as a models. The black box models apply curve fitting directly to the map variables (Π_c, $\bar{W}$, $\bar{N}$ and η_c) to produce a model. The modeling effort is then to create functions describing the speed lines and iso-contours of efficiency of the map.

The following two subsections present examples of black and gray box models, that serves and an indication of from where inspiration to the models developed in this thesis have come from. It should not be seen as an exhaustive summary of all available models. Compressor flow and efficiency are commonly modeled separately. This separation is also chosen here, and examples of compressor flow models are presented first, followed by examples of compressor efficiency models. The models should show the vast range of modeling approaches and complexity levels, where some models are especially designed for a certain purpose, while others are meant to be more general. The last section presents the Ellipse compressor model developed in this thesis, and overviews the small differences of the models used in the different appended papers.

3.4.1 Examples of compressor mass flow models

In [111, p.73] an S-shaped characteristics is proposed as

$$\Psi_c = \Psi_{c,0} + c_H \left(1 + \frac{3}{2} \left(\frac{\Phi_c - c_W}{c_W} \right) - \frac{1}{2} \left(\frac{\Phi_c - c_W}{c_W} \right)^3 \right) \tag{3.9}$$

where the model parameters c_W and c_H are referred to as "semi-width" and "semi-height", respectively. The same model is used also in e.g. [17, p.136], [139, p.1644] and [146, p.816]. In [139] the following two model modifications are proposed, to better describe the "skewness" of the characteristics

$$\Psi_c = \Psi_{c,0} + H \sin\left(\frac{\pi}{2}\frac{\Phi_c - c_W}{c_W}\right) \tag{3.10}$$

$$\Psi_c = \Psi_{c,0} + c_H\left(\sin\left(c_2\frac{\Phi_c - c_W}{c_W}\right) + c_3 \sin\left(\frac{c_2}{c_4}\frac{\Phi_c - c_W}{c_W}\right)\right) \tag{3.11}$$

where the second equation is referred to as the "two-sine"-model. A three region flow model is proposed in [73, p.392]. The model is formulated in dimensionless pressure rise ($\tilde{C} = {}^{\Delta p_c}/_{1/2\rho U^2}$), and dimensionless flow ($\dot{\tilde{m}} = {}^{C_x}/_{U} = {}^{W_c}/_{\rho A U_c}$) as

$$\tilde{C}_{mod} = \begin{cases} b_2\dot{\tilde{m}}^2 + b_0 & W_c < 0 \\ c_3\dot{\tilde{m}}^3 + c_2\dot{\tilde{m}}^2 + c_0 & 0 \le W_c \le W_{c,\mathrm{ZS}} \\ d_3\dot{\tilde{m}}^3 + d_2\dot{\tilde{m}}^2 + d_1\dot{\tilde{m}} + d_0 & \text{else} \end{cases} \tag{3.12}$$

The same model was used slightly modified in [129], where $b_0 = c_0$ are given by (3.2), and 2D interpolation in map data was instead proposed for $W_c > W_{c,\mathrm{ZS}}$. In [177, p.247] a model with two flow regions is proposed as

$$\Delta p_c = \begin{cases} \frac{\rho U^2}{2}\left[c_1 \arctan[c_2(\Phi_c - c_3)] + f(\Phi_c)\right] & \text{if } \Phi_c > \Phi_{c,lim} \\ c_4 + c_5\Phi_c^2 & \text{else} \end{cases} \tag{3.13}$$

where $f(\Phi_c)$ is a third order polynomial in Φ_c. The low flow part is referred to [73].

The following model based on affine functions in the Mach number is proposed in [83]

$$\Psi_c = \frac{k_1 + k_2 M_c + k_3\Phi_c + k_4\Phi_c M_c}{k_5 + k_6 M_c - \Phi_c} \tag{3.14}$$

The model is also used in e.g. [22, p.392] and [122, p.385]. Quadratic functions in M_c, instead of affine functions, are proposed in [126, p.5] to improve the model accuracy. Another extension to (3.14) is presented in [107] where again affine functions were used, but now for each compressor speed line SpL. Linear interpolation is then performed between the two SpL models that delimits a zone in the map to ensure continuity. In [40] and [41], the model from [107] is extended with thoughts from [44], utilizing quadratic functions in M_c for each SpL instead of affine. Interpolation between SpL models are used, which is said to give good performance for more than ten maps tested, see [40, p.366]. A physical model is presented in [117, p.2-3], and it is simplified to a black box model as

$$\Pi_c = \left(\frac{U_2^2\left[B\left({}^{W_c}/_{U_2}\right)^2 + C\left({}^{W_c}/_{U_2}\right) + D\right]}{c_{p,c}T} + 1\right)^{{}^{\gamma_c}/_{(\gamma_c - 1)}} \tag{3.15}$$

where $B = b_0 + b_1 U_2 + b_2 U_2^2$, $C = \frac{2 \cdot B \cdot W_{c,\mathrm{ZSL}}}{U_2}$, $D = d_0 + d_1 U_2 + d_2 U_2^2$. Mass flow at the zero slope line is explicitly modeled as $W_{c,\mathrm{ZSL}} = e_0 + e_1 U_2 + e_2 U_2^2$. The model is said to be validated on three automotive sized compressors with good accuracy. The following model is proposed in [72, p.64]

$$\Pi_c = C_3 - C_2 \left[\bar{W} - C_1\right]^2 \tag{3.16}$$

where C_i, $i \in \{1, 2, 3\}$ are polynomials in ω_{tc}. Citing an internal Ford document, the so called Zero Slope Line Method (ZSLM) is presented in [112, p.6], and compared to two other models (of which the model (3.14) is one). Two model regions are defined, one for flows left of the zero slope line ZSL, and one for flows right of the ZSL

$$\frac{\Phi_c}{\Phi_{c,top}} = \begin{cases} 1 + c_6 e^{-(c_7 N_{\mathrm{tc}})} \left(1 - e^{c_5 \left(\Pi_c / \Pi_{c,\mathrm{ZSL}} - 1\right)}\right) & \Phi_c > \Phi_{c,top} \\ 1 - c_6 e^{-(c_7 N_{\mathrm{tc}})} c_5 \left(\Pi_c / \Pi_{c,\mathrm{ZSL}} - 1\right) & \text{otherwise} \end{cases} \tag{3.17}$$

where $\Phi_{c,top}$ and $\Pi_{c,\mathrm{ZSL}}$ are given by

$$\Phi_{c,top} = c_1 N_{\mathrm{tc}} + c_2 N_{\mathrm{tc}}^2 \tag{3.18}$$

$$\Pi_{c,\mathrm{ZSL}} = c_3 + c_4 \Phi_{c,top}^2 \tag{3.19}$$

and are said to make up a line through the maximum mass flow points of each SpL. Though from the name of the model, and from the further presentation of the model, this seems to refer to the line through the maximum pressure ratio point of each SpL. A surge focused model is proposed in [66, p.1289-1290] as

$$\Pi_c = c_0 + c_1 W_c + c_2 W_c^2 + c_3 W_c^3 \tag{3.20}$$

where c_i, $i \in \{0, 1, 2, 3\}$ are third order polynomials in N_{tc}, which were said to be needed for the compressor studied. For the small region in the compressor map, usually encountered in normal engine operation, following model is proposed in [48, p.134]

$$W_c = c_5 \tilde{\Pi} + c_6 \tilde{\Pi}^2 + c_7 \tilde{\Pi}^3 \tag{3.21}$$

where $\tilde{\Pi} = \Pi_c - c_3 \tilde{N} - c_4 \tilde{N}^2$, and $\tilde{N} = \frac{N_{\mathrm{tc}} - c_1}{c_2}$. In [6, p.110] the following elliptic model structure is proposed

$$\Phi_c = \sqrt{\frac{1 - c_1 \Psi_c^2}{c_2}} \tag{3.22}$$

where c_i are fitted minimizing the total least squares of $\Psi_c^2 c_1 + \Phi_c^2 c_2 = 1$. In [163] the following model structure is proposed

$$\Psi_c = c_0 + c_1 \Phi_c + c_2 \Phi_c^2 + c_3 \Phi_c^3 \tag{3.23}$$

to model surge in a bi-turbo engine. An ellipse like model is proposed in [168, p.975] as

$$\Phi_c = \sqrt{\max\left(0, \frac{1 - C_2 \left(\Psi_c - c_3\right)^2}{C_2}\right)} + c_4 \tag{3.24}$$

where C_1 and C_2 are second order polynomials in ω_{tc}.

3.4.2 Examples of compressor efficiency models

An efficiency model parametrized as a function of Φ_c and M_c is presented in [83] as

$$\eta_c = \frac{c_{1,0} + c_{2,0}M_c}{c_{3,0} - M_c} + \frac{c_{1,1} + c_{2,1}M_c}{c_{3,1} - M_c}\Phi_c + \frac{c_{1,2} + c_{2,2}M_c}{c_{3,2} - M_c}\Phi_c^2 \tag{3.25}$$

The same approach is used in e.g. [22, p.393] and [126, p.5]. In [72], an efficiency model with six parameters are proposed as

$$\eta_c = c_1 - \chi^T Q \chi \tag{3.26}$$

where $Q = [c_2 \ c_3; \ c_3 \ c_4]$, and $\chi = \left[\bar{W} - c_5; \ \Pi_c - c_6\right]$. The parameter c_6 is interpreted as the maximum efficiency, and c_5 and c_6 then give the location in $\bar{W}$ and Π_c of the maximum efficiency point. The parameters c_{2-4} give elliptic shaped contours of constant efficiency. A small modification is proposed in [6, p.113] where the definition of χ is changed in $\chi = \left[\bar{W} - c_5; \sqrt{\Pi_c - 1} - (c_6 - 1)\right]$. The definition of χ was modified also in the efficiency model presented in [168, p.974-975], where $\chi = \left[\bar{W} - c_5; (\Pi_c - 1)^{c_7} - \left(c_6 - 1\right)^{c_7}\right]$, and c_7 is introduced as an extra tuning parameter. In [152, p.3] and [47, p.152] a six parameter efficiency model is proposed as

$$\eta_c = c_1 + c_2 N_{\text{tc}} + c_3 N_{\text{tc}}^2 + c_4 W_c + c_5 W_c^2 + c_6 W_c N_{\text{tc}} \tag{3.27}$$

By utilizing models for isentropic work, and models for actual work, the following eight parameter efficiency model is proposed in [48]

$$\eta_c = \frac{U_2^2 \left(c_1 + c_2 \left({}^{W_c}/_{U_2}\right) + c_3 \left({}^{W_c}/_{U_2}\right)^2\right)}{c_4 + c_5 W_c + c_6 U_2 + c_7 W_c U_2 + c_8 U_2^2} \tag{3.28}$$

Many MVEM mainly uses an η_c-model to calculate the compressor torque Tq_c, and a model for Tq_c is proposed in [129]

$$Tq_{c,mod} = N_{\text{tc}} \frac{p}{\sqrt{T}} \left(c_1 W_c \frac{\sqrt{T}}{p} + c_2\right) \tag{3.29}$$

which is said to be valid from choke flow down to zero flow. For negative flow it is further proposed to simply continue extrapolating the above model. An efficiency model was presented in [107] (and also used in [41] and [40]). The model relies on a compressor flow model that extends the model (3.14). Given a specific flow, the flow model is then used to calculate a modeled Π_c, and this is used to calculate a specific enthalpy gain through the compressor. A specific isentropic enthalpy gain $\Delta h_{is,m}$ is then modeled as affine function in W_c for each speed. The efficiency model is given by

$$\eta_c = \frac{c_{p,c} T \left(\Pi_c^{(\gamma_c - 1)/\gamma_c} - 1\right)}{C_1(N_{\text{tc}}) - C_2(N_{\text{tc}}) W_c} \tag{3.30}$$

where the nominator is Δh_m and the denominator is $\Delta h_{is,m}$, and C_1 and C_2 are second order polynomials in N_{tc}. In [122] the following nine parameter efficiency model is proposed

$$\eta_c = C_0 + C_1\Phi_c + C_2\Phi_c^2 \tag{3.31}$$

where C_{0-2} are three second order polynomials in M_c.

3.5 The Ellipse compressor model used in Papers 1, 4 and 5

Following the brief examples of related compressor models available in the literature, this section presents and discusses the Ellipse compressor model. The resulting model gives an S-shaped characteristic, where an approximate elliptic shape describes most of the normal operating range. The modeling effort is divided in three main regions in flow for a given speed.

The model is formulated in the corrected quantities of the compressor map, and the correction equations, see equations (2.3) and (2.5), are used to handle variations in compressor inlet conditions. The model describes the pressure ratio the compressor can maintain given an operating point in corrected flow $\bar{W}$ and corrected compressor speed $\bar{N}$ as

$$\hat{\Pi} = f_{\hat{\Pi}}(\bar{W}, \bar{N})$$

The model follows the Moore-Greitzer approach and introduces a compressor mass flow state as (3.1), i.e.

$$\frac{dW_c}{dt} = \frac{\pi d_c^2}{4L_c}\left(\hat{p}(\bar{W}, \bar{N}) - p_{02}\right)$$

where d_c and L_c are constants and $\hat{p} = \hat{\Pi}{\cdot}p_{01}$ is the modeled compressor pressure build up. The compressor inlet pressure p_{01} and outlet pressure p_{02} are given by the surrounding components. The mass flow state enables surge simulation, and is further used to change the causality of the model calculations. Instead of having a pressure ratio and speed defining a flow, the model calculates a pressure build up $\hat{p}$ given an operating point in $\bar{W}$ and $\bar{N}$. This is beneficial since most maps have a uniquely defined Π_c for given $\bar{W}$ and $\bar{N}$. This uniqueness is not necessarily found for all measured maps, and slightly backward bending speed lines were found in the analysis of compressor maps in Paper 5, where a reduction in $\bar{W}$ was seen for Π_c below the choking point pressure ratio $\Pi_{c,\mathrm{Ch}}$. The reduction in $\bar{W}$, i.e. the amount of backward bending, was though very limited. Further, the extra mass flow state means that a measured Π_c and $\bar{W}$ must deviate from $\hat{\Pi}$ and $\bar{W}$ during transients.

Given a $\bar{N}$, a number of characteristic points define a modeled speed line SpL, and an overview of these characteristic points of a SpL is shown in Fig. 3.5. Following the SpL from left to right, three main regions can be defined. Negative flow and up to zero flow is modeled using a polynomial in Paper 1, while a

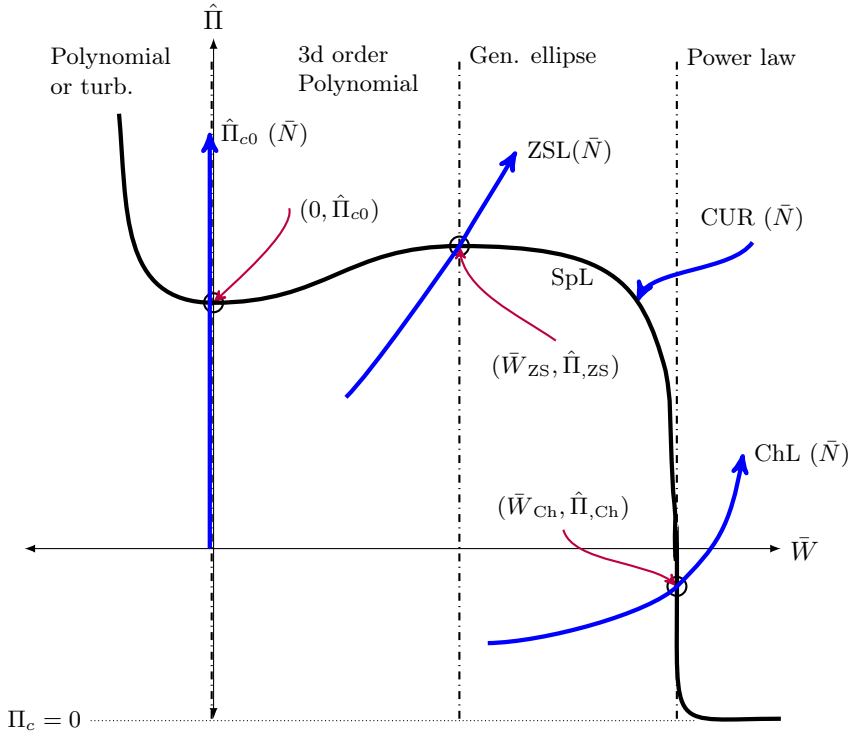

Figure 3.2: Overview of the Ellipse compressor model.

turbine flow like parabola model is used in Paper 4. In both papers the modeled SpL passes through the zero flow pressure build up point $(0, \hat{\Pi}_{c0})$. For Paper 5 no description for negative flow is implemented. From zero flow to the Zero Slope Line ZSL, found close to the surge line, a third order polynomial is used as a model. The polynomial is parametrized to give zero slope at zero flow and at the ZSL, and this part of a SpL is commonly referred to as the unstable branch. For flows from the ZSL to the choke line ChL, where the SpL has infinite slope, a generalization of an ellipse is used as a model. It should be noted though, that the curvature of the modeled ellipse is not necessarily equal to two, and a true mathematical ellipse does hence not result. For model implementations where the choking pressure ratio is larger than zero, also a fourth region is used for simulation purposes. A power law model is then used that converges asymptotically to $\hat{\Pi} = 0$ for infinite $\bar{W}$.

Descriptions of $\hat{\Pi}_{c0}(\bar{N})$, $\mathrm{ZSL}(\bar{N})$ and $\mathrm{ChL}(\bar{N})$ are key components of the model. These descriptions differed some between the papers, and the differences are described in the following. The compressor modeling of Paper 1 was based on data from four compressor maps, and polynomials were used to model $\hat{\Pi}_{\mathrm{ZSL}}$ (through 1 for $\bar{N} = 0$), $\bar{W}_{\mathrm{ZSL}}$ (through 0 for $\bar{N} = 0$), CUR, $\bar{W}_{\mathrm{ChL}}$ and $\hat{\Pi}_{c0}$, while a zero choking pressure ratio was modeled i.e. $\hat{\Pi}_{\mathrm{ChL}} = 0$.

Data from 236 compressor maps were used in Paper 4. $\hat{\Pi}_{\mathrm{ZSL}}$ and $\bar{W}_{\mathrm{ZSL}}$ were

modeled using power laws through 1 and 0 for $\bar{N} = 0$, respectively. $\hat{\Pi}_{c0}$ was further modeled using $\Gamma_{\Pi_{cs}}$, an affine model described $\bar{W}_{\text{ChL}}$, and a constant $\hat{\Pi}_{\text{ChL}} = 0$ was assumed. The curvature was divided into two models, utilizing an affine model and a power law model respectively.

For Paper 5, a total of 305 compressor maps were used in the modeling. The models for $\hat{\Pi}_{\text{ZSL}}$ and $\bar{W}_{\text{ZSL}}$ from Paper 4 were used. Power law models were then used for $\bar{W}_{\text{ChL}}$, $\hat{\Pi}_{\text{ChL}}$ and $\hat{\Pi}_{c0}$. A second order polynomial function in $\bar{N}$ was used to describe CUR.

To exemplify, the ellipse part of the final model from Paper 5 is presented here

$$\hat{\Pi}_{mod} = \left(1 - \left(\frac{\bar{W} - \bar{W}_{\text{ZSL}}}{\bar{W}_{\text{ChL}} - \bar{W}_{\text{ZSL}}}\right)^{\text{CUR}}\right)^{\frac{1}{\text{CUR}}} \cdot \left(\hat{\Pi}_{\text{ZSL}} - \hat{\Pi}_{\text{ChL}}\right) + \hat{\Pi}_{\text{ChL}} \quad (3.32)$$

where $\bar{W}_{\text{ZSL}}$, $\bar{W}_{\text{ChL}}$, $\hat{\Pi}_{\text{ZSL}}$, $\hat{\Pi}_{\text{ChL}}$ and CUR are all functions of $\bar{N}$. With the gas state at the compressor inlet given, i.e. T_{01} and p_{01} and the corresponding reference states, the corrected mass flow $\bar{W}$ is calculated from (2.3) using the model state W_c given by (3.1). The corrected compressor speed $\bar{N}$ is calculated using (2.5). The Ellipse model then gives $\hat{\Pi}_{mod}$, and $\hat{p}$ of (3.1) is then calculated as $\hat{p} = \hat{\Pi}_{mod} \cdot p_{01}$.

The efficiency model in Papers 1, 4 and 5, is based on the model from [72], with the extension from [6]. However, the efficiency model uses a lower saturation threshold as

$$\eta_{c,mod} = \max\left[\eta_{c,\text{lower sat.}},\ c_1 - \chi^T Q \chi\right] \quad (3.33)$$

where $Q = [c_2\ c_3;\ c_3\ c_4]$, and $\chi = \left[\bar{W} - c_5; \sqrt{\Pi_c - 1} - (c_6 - 1)\right]$. By selecting the same threshold for both surging and choking flows, a continuous efficiency model results. The threshold was commonly set to $\eta_{c,\text{lower sat}} = 30\%$.

Given an operating point in $\bar{W}$ and Π_c, the modeled $\eta_{c,mod}$ can be calculated, and a modeled compressor discharge temperature $T_{02,mod}$ can be calculated using $\eta_{c,mod}$ in (2.6) given T_{01} and Π_c. The modeled compressor power $P_{c,mod}$ is then given by

$$P_{c,mod} = W_c c_{p,c} (T_{02,mod} - T_{01}) \quad (3.34)$$

and the loading compressor torque of (2.1) is given by

$$Tq_{c,mod} = \frac{P_{c,mod}}{\omega_{tc}} \quad (3.35)$$

Some further comments to the model can be given. Since the surge line is a system property, no surge line is defined in the model. A temperature rise in the control volume before the compressor during surge, is described by the model for negative flow. However, no temperature rise at the compressor inlet will result for operation with flows close to the surge line, i.e. recirculation. The compressor model acts as a turbine during the reverse flow periods of surge, and for operation at pressure ratios of less than unity with positive flow.

4

Experimental setups

This chapter presents the sensory equipment and measurement systems of two of the experimental setups that have been used, and details some of their characteristics: the engine test stand at Vehicular systems (measurements for Papers 1, 2, 3 and 4), and the Saab Trollhättan gas stand (Papers 3 and 5). Sensor installation details, and details of the sensors used will be presented. The surge test stand, used for some of the surge measurements (Papers 1 and 4) is not presented here, and the interested reader is instead referred to [5] for details.

For general information on common automotive sensors, the reader is referred to e.g. [102] and [171]. A good overview of measuring pressure and temperature in a turbo is found in [148].

4.1 The engine laboratory at Vehicular Systems

The engine laboratory consists of one engine test cell, equipped with two engine test stands. The engines of each test stand are connected to individual Schenck Dynas3-LI250 electric dynamometers from 2002 (rated speed of 10krpm, rated power of 250kW, and rated torque of 480Nm). The electric dynamometers load the engines, and also act as the start motors. The electricity the dynamometer generates, is fed back to the electric grid, and the heat expelled by the engine to the coolant system, supports the heating of the university buildings.

The laboratory equipment and setup are subject to continuous development, and data from four different engine installations have been used for this thesis. Some main characteristics of the engines are presented in Table 4.1. An installation photo of the series sequentially turbocharged LNF engine is shown in Fig. 4.1, where the low pressure stage and the high pressure stage are marked. The two white rolled up cables are connected to the two turbo speed sensors.

Engine	Description
B235R	Saab, 2.3L, 230hp, 350Nm, fixed cams, single stage turbocharger, MHI TD04HL-15T
L850	Saab/GM (B207R), 2.0L, 210hp, 300Nm, extended with dual variable cam phasing, single stage turbocharger, MHI TD04L-14T
LNF	GM, 2.0L, 265hp, 350Nm, dual variable cam phasing, twin-scroll single stage turbo, BW K04-2277
LNF-TS	GM, 2.0L, dual variable cam phasing, series sequential two-stage turbo system extended with actively controlled high pressure stage compressor by-pass, BW K04-2270 + BW KP35-1574

Table 4.1: Main characteristics of the four different engine installations. All engines are water cooled four cylinder inline spark ignition engines with a single air-to-air intercooler, and 16 valves. Fuel used is petrol.

The packaging constrains the sensor installation, which can affect the measurements.

The engine control system is based on a dSPACE MicroAutoBox (MABx) and RapidPro (RP) architecture. The engine control system is a large Simulink model, that is compiled using Real Time Workshop. The generated code is then executed in real time on the MABx. The can directly control any of the actuator signals.

The test cell measurement system consists of an HP VXi system, with an HPE1415A module and an HPE1433A module. The HPE1415A module is used to measure analog and digital signals, with a sample frequency of up to 2000Hz, and has built in support for thermocouples. The HPE1433A module is a fast 8 channel converter with separate A/D-converters for each channel. The HPE1433A is used with a sampling frequency of up to 192kHz, and can also be used to sample in the crank angle domain.

The signals are measured by the HP VXi system. Commonly, a sampling frequency of 1000Hz is used for the HPE1415A and 128kHz is used on the HPE1433A. The dSPACE control system is also used to measure, where all engine production sensors and actuator signals can be sampled, along with a large number of extra digital and analog signals. On the dSPACE system, commonly a sampling frequency of 80Hz is used, which is equivalent to one of the main control loops of the engine control system. A summary of the measurement systems is presented in Table 4.2.

Most measurements conducted in the engine test stand for this thesis were for stationary engine operating points. For each operating point measured, the system was allowed time to stabilize all components thermally, and a mean value of 10s of each signal was then calculated and stored. The surge oscillations presented in Paper 1 and Paper 4 are typically phenomena with a corresponding frequency of approximately 10Hz, and a sampling frequency of at least 1000Hz was used for these measurements .

The next subsections will discuss the sensors and their installation, and for further information on the engine test stand the reader is referred to [6, p.217-].

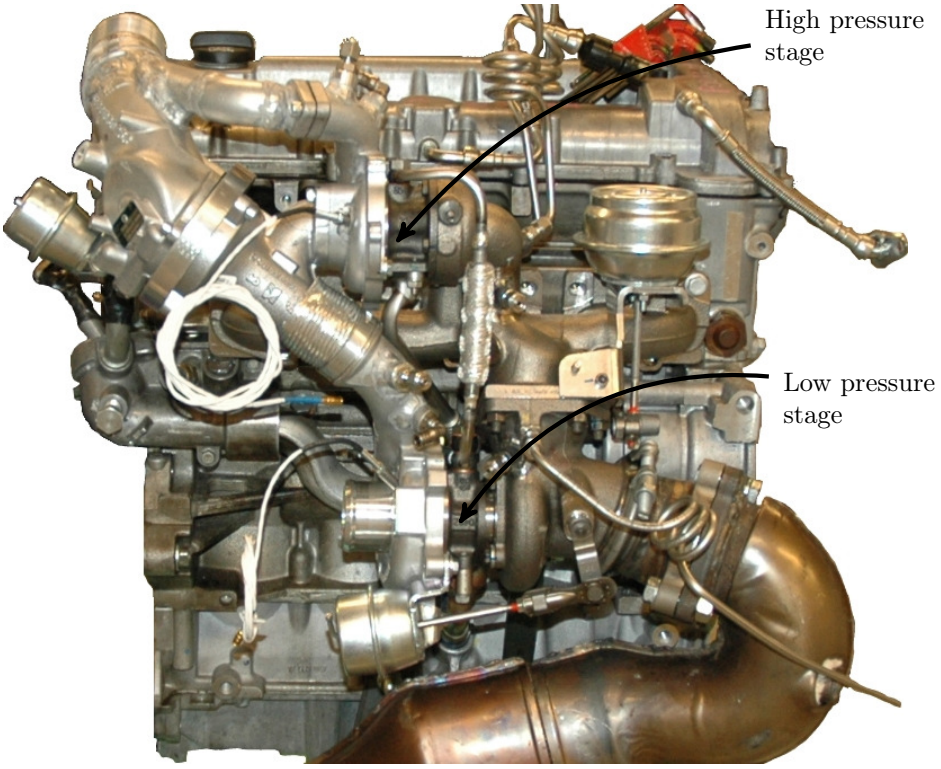

Figure 4.1: Photo of the LNF engine with the two stage series sequential turbo system.

4.1.1 Sensors

This section presents the typical sensors used during the experiments in the engine test stand: temperature T, pressure p, mass flow W, and turbo speed N_{tc}. The final subsection summarizes some of the other sensors mainly used for diagnostic purposes. An example of the locations of different sensors used in Paper 3 is shown in Fig. 4.2, and an actual photo of the same experimental setup is shown in Fig. 4.3.

Temperature

All temperature sensors are IEC class 1 K-type thermocouples from Pentronic, and the same thermocouple extends from the measurement location to the measurement system i.e. no connection cables of other materials are involved in the thermocouple circuit. Class 1 K-type thermocouples have an accuracy of $\pm 1.5^o\text{C}@T \in [-40, 375]^o\text{C}$ and $\pm 0.004 \cdot |T|@T \in [375, 1000]^o\text{C}$, see e.g. [115, p.574] and [125, Ch.3:4]. The sensors are all shielded, and the width of the sensor bodies are mostly 3mm. The compressor outlet temperature sensors (e.g. T_{02} of Fig. 4.2) for the series sequential installation used a sensor width

Model	Description
HP VXI, HPE1415	64-channel algorithmic closed loop controller. 16-bit A/D-resolution, up to 56kSa/s maximum reading rate dependent upon configuration. 64kSa measurement FIFO memory built in. Installed modules of the VXI system are: HPE8400A, HPE8491A, 3xHPE1503A, HPE1505A, HPE1537A, and HPE1538A.
HP VXI, HPE1433	8-channel 196kSa/s digitizer (+DSP) with integrated sensor signal conditioning, anti-aliasing protection, digitization and high-speed measurement computation. 32Mb of RAM. Separate A/D converters.
MABx/RP	dSPACE Microautobox (MABx) and RapidPro-system (RP). The RP consists of four layers; two powerstage layers for output handling, one control unit layer capable of both input and output, and one signal conditioning layer for sensor input.

Table 4.2: Summary of the measurement systems in the engine laboratory of vehicular systems. The control system of the engine is a compiled Matlab Simulink model, that is run in real time on the dSPACE equipment (MABx/RP). All actuator control signals can also be sampled using the MABx/RP.

of 1.5mm. Most sensors are from 2008, but some 3mm sensors were from 2003. The temperature sensor T_{LFE3} is used by the LFE3 mass flow sensor, and is also 3mm in width.

During the measurements for this thesis, the sensor tips were adjusted to be close to the pipe center for each measurement location. Due to packaging constraints, mostly only single temperature sensors were fitted for each locations. Three sensors were used for the compressor inlet temperature measurement in Paper 2 and Paper 3. Ice water and boiling water were used to calibrate the temperature sensors, before the measurement series. The recovery factor used to calculate the total temperature from a measured temperature [8, p.44], is assumed to be 1. This means that the measured temperature is assumed to be the total temperature. The pulsations caused by the cylinder pumping of the engine, was not considered to cause significant oscillations in the control volumes surrounding the compressor. Most measurements are also stationary engine operating points. The temperature signals during compressor surge were not explicitly used in the modeling. For the turbine side measurements in Paper 2, only small Π_t was measured, and the oscillations in pressure were hence comparable small.

Pressure

The pressure sensors are all but one from Kistler, and of either the 4260-series (4260A50 340kPa and 4260A75 500kPa piezoresistive absolute pressure sensors, 0.05% Full Scale (FS) accuracy, 0.1% FS stability per year, 3xFS proof pressure, $f_{max} = 2$kHz) or the 4295-series (4295A2 and 4295A2V, 200kPa absolute pressure sensors). The absolute pressure sensor p_{LFE3} measured internally by the LFE3 mass flow sensor system, is manufactured by Micro Switch Honeywell.

The sensors for the compressor inlet pressure measurement in Paper 2 and Paper 3 ($p_{01,1}$, $p_{01,2}$ and $p_{01,3}$ in Fig. 4.2), are placed on a straight pipe, following an air filter to reduce flow disturbances. Four pressure taps are connected together, and the sensors $p_{01,1}$ and $p_{01,2}$ are connected to the four taps. The $p_{01,3}$-sensor in Fig. 4.2 uses a single pressure tap, due to packaging constraints.

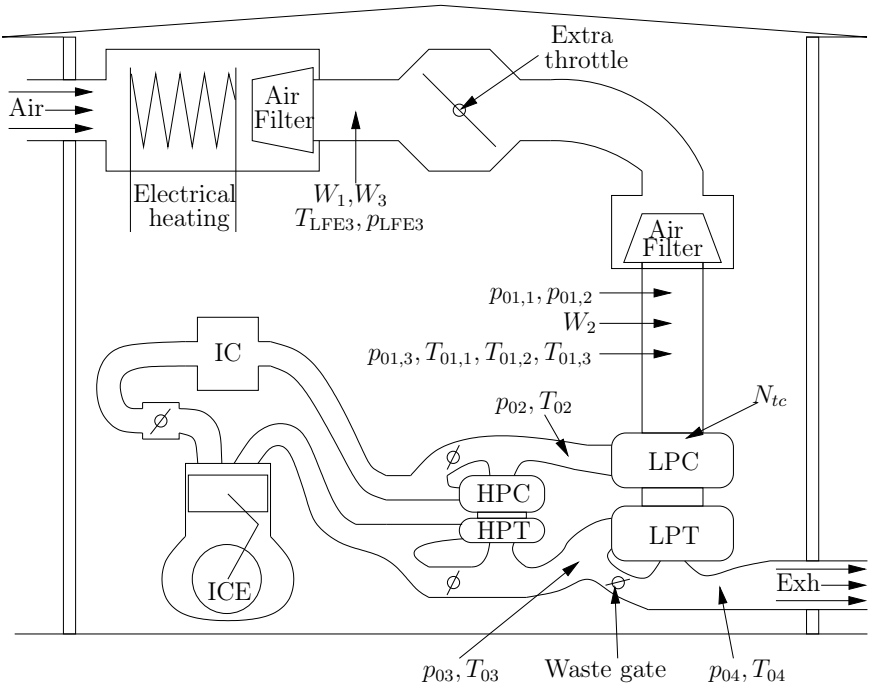

Figure 4.2: Schematic picture of the experimental setup used in Paper 3. The electrical heating section is removed when not required. The extra throttle is used to decrease compressor inlet pressure, and the throttle is controlled using the engine control system (MABx/RP). The air filters are used to straighten the air flow for the mass flow and pressure measurement locations. Air comes in from the left, runs through the compressor inlet variation rig, goes through the compressor stages, the engine, the turbine stages, catalyst, muffler and are expelled to the right.

The positioning of the pressure taps for p_{02}, p_{03} and p_{04} are also restricted due to the packaging, but placed at the most straight sections of the respective pipes. The exhaust side pressure sensors, p_{03} and p_{04}, are mounted on spiral shaped pipes approximately 0.50m in length, due to restricted temperature limits of the sensors. Also the cold side temperature sensors are typically mounted with connecting hoses, and only the intake manifold pressure is flush mounted. Measured pressures were assumed to be the static pressures. Total pressures are then calculated from each pressure measurement using the measured mass flow, measured temperature and the pipe area as

$$p_0 = p + \frac{\rho \cdot v^2}{2} = p + \frac{W^2}{2 \cdot \rho \cdot A^2}$$

where p_0 is the total pressure, p the measured pressure, v the flow velocity, ρ gas density, W measured mass flow, and A the cross sectional area at the measurement location. The difference between p_0 and p is the dynamic pressure,

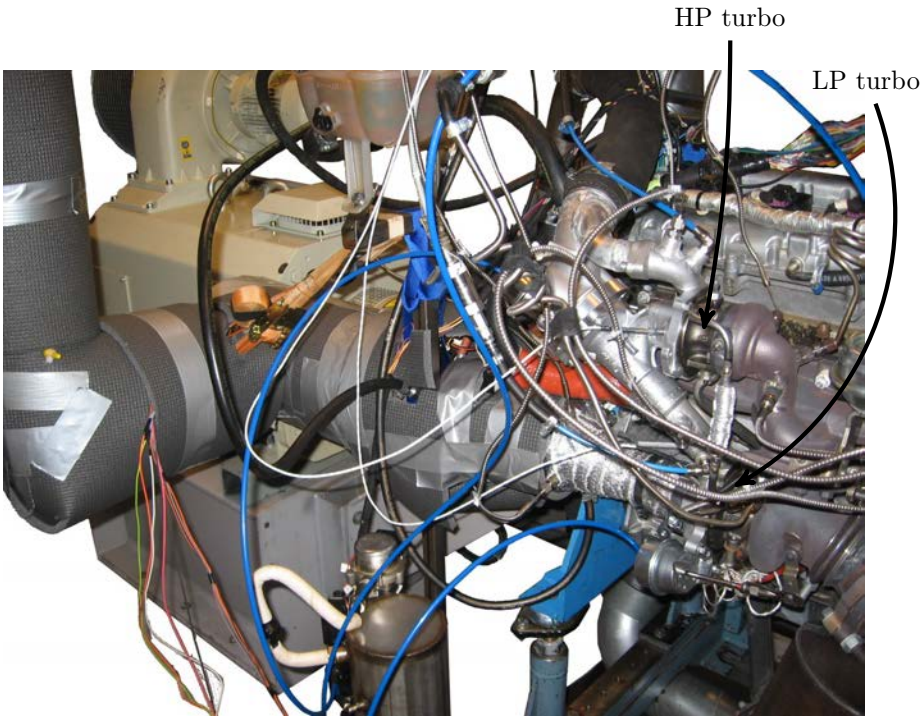

Figure 4.3: The compressor inlet condition variation rig, the Schenk dynamometer and the engine test stand with the two stage system mounted on the LNF engine. The high pressure turbo (HP) and the low pressure turbo (LP) are marked.

describing the increase in pressure that the gas experiences when it is brought to stand still. A reference sensor is used to calibrate the pressure sensors before a measurement series, to minimize any offset errors between the sensors. Further, all pressure sensors are measured at engine off conditions, both before and after each measurement sequence, to indicate any sensor drift during the measurements. Most investigations are conducted on the compressor side, where the oscillations in pressure due to the engine pumping are far less severe, and the engine is typically operated in stationary conditions (except for the surge measurements). Turbine inlet and outlet pressures are measured in Paper 2. However, the range in measured Π_t was limited due to the indirect measurement of turbine flow (compressor flow and fuel flow calculated using λ) and the limited spring pre-tension of the waste-gate valve (where the WG opens for large differential pressure across the turbine). The potential measurement errors due to pulsating flow was therefore considered neglectable.

Mass flow

For Paper 2 and Paper 3, three different mass flows are measured. W_1 in Fig. 4.2 is measured using the LFE3 system. The LFE3 sensor system is purpose built for automotive research by the Technical University of Denmark (DTU), and uses the differential pressure principle. The differential pressure is measured over a laminar flow element, that gives the volumetric flow. T_{LFE3} and p_{LFE3} are then used to calculate the density, and the mass flow is determined according to $W_1 = \dot{V} \cdot \rho_{\mathrm{LFE3}}$, where $\dot{V}$ is the volumetric flow and ρ_{LFE3} is the density at the measurement location. The LFE3 differential pressure sensor is a 164PC0137 from Micro Switch Honeywell. The mass flow sensor W_2 in Fig. 4.2 is a Bosch production sensor, based on the hot-wire principle producing a digital signal. An extra differential pressure sensor is for diagnosis purposes mounted in parallel with the LFE3 differential pressure. The mass flow W_3 in Fig. 4.2 is calculated from also this differential pressure sensor, using the T_{LFE3} and p_{LFE3} to calculate the air density. This extra differential pressure sensor is a Kistler 4264AB03-sensor (bi-directional differential pressure sensor, $\pm$17kPa, 0.2(0.05)% FS accuracy, 0.1% FS stability per year, 3xFS proof pressure, f_{max} = 2kHz). The differential pressure based sensor was installed approximately 1.5m of piping upstream of the compressor, and the hot wire sensor was approximately 0.5m upstream.

Here, mass flow was measured at two different locations and calculated from three sources. The mass flow measurement stations were located on approximately 0.5m straight pipe sections immediately downstream of an air filter, to make the air flow as uniform as possible within the packaging constraints of the test stand. For stationary measurements, the distance from the sensor to the location were the measurement is desired causes no problem, since in stationarity these flows will be equal. The mass flow signal measured during surge was not considered reliable.

Misc sensors

The turbo speed N_{tc} of Fig. 4.2 is measured using an Acam PicoTurn BM-V6 (range $0.2 - 400$krpm) system, using a ferrite core coil to sense a passing blade through change in inductance by eddy currents. The actual sensor installation can be seen in Fig. 4.1, where the rolled up white cables lead up the sensors mounted on each compressor housing. The BM-V6 system is capable of both analog and digital output signal, where the latter is used to reduce noise sensitivity. The speed sensor position is adjusted using the built in sensor positioning functions of the BM-V6, to ensure a good quality of the turbo speed measurement. The LNF engine is equipped with AVL GU21D cylinder pressure sensors, which were delivered newly calibrated with the engine in 2007. Waste-gate positions on the LNF two-stage turbo system was measured using Gill Blade 25 sensors ($0 - 25$mm, f_{max} = 1kHz, 125^{o}C max temperature). The installation required extra purpose built cooling systems. The Schenk dynamometers are equipped with GIF F1 (rated torque 650Nm, max speed 12krpm) torque sensors. LeineLinde crank angle sensors were used, with a resolution of 720 points per engine revolution.

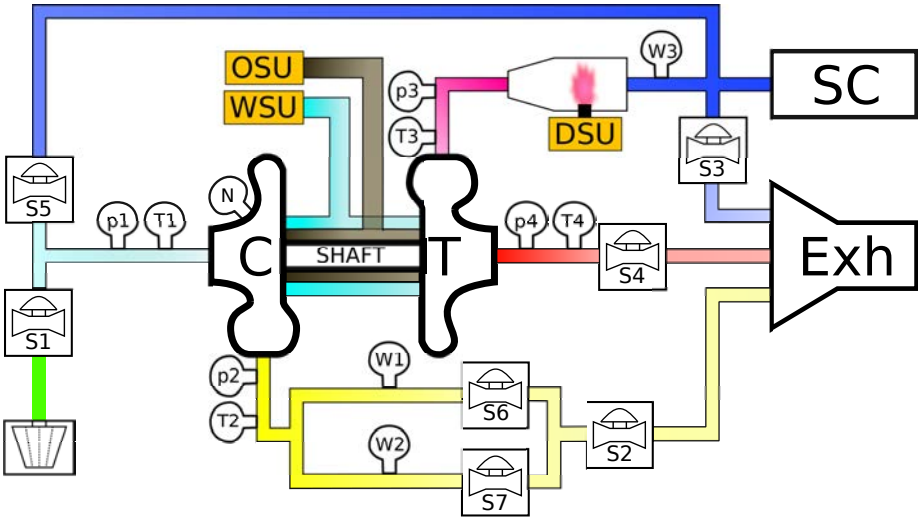

Figure 4.4: Schematic overview of the Saab gas stand. The abbreviations are: C compressor, T turbine, SC screw compressors, Exh exhaust chimney, DSU/OSU/WSU diesel/oil/water supply unit respectively, and S are valves to control flow. p, T, W, and N indicate measurement locations.

4.2 Saab Trollhättan gas stand

The extended maps presented in Paper 5 were measured at Saab Powertrain in Trollhättan, Sweden. As an unfortunate side note, the measurements conducted for Paper 5 were probably among the last ever to be made in the gas stand in Saab's name, as Saab was soon afterward declared bankrupt. The gas stand equipment is delivered by AVL. Two Atlas Copco ZR90VSD screw compressors (water cooled variable speed drives) deliver pressurized oil free air, that is being conditioned using an air-to-water intercooler. The air can be delivered to both compressor and turbine. A diesel burner is used to increase turbine gas flow temperature. Turbo oil and water supply can be controlled, both feeding pressure and temperature. The p_{oil}/T_{oil} and p_{water}/T_{water} circuits are individually controllable. The climate of the gas stand room is controlled. An overview of the gas stand is shown in Fig. 1, and actual gas stand installation photos (for the Paper 5 measurements) are shown in Fig. 4.5.

For further details on the gas stand setup, the interested reader is referred to e.g. [92] and [173].

4.2.1 Measurement equipment

The most important parts of the AVL data acquisition system were four F-FEM-AIN modules for analog, and two F-FEM-CNT modules for digital signals. The measurement stations for $T_{0i},\ i = \{1, 2, 3\}$ were equipped with 8 sensors each. The sensors were divided into two groups of four sensors, spread

out evenly circumferential around the measurement planes for redundancy and diagnostic purposes. PT100 sensors were used for the cold temperatures, and the documentation of the sensors stated $T_{max} = 300^o$C and an accuracy of $\pm(0.15 \pm 0.002T)^o$C. Eight sensors were used to measure T_{01}, and eight sensors were used for T_{02}. Pentronic K-type thermocouples were used in the hot flows, with $T_{max} = 1333^o$C and a stated relative accuracy is $< 0.75\%$. The compressor side pressures, p_1 and p_2, were relative pressure sensors, with a range of $\Delta p \in [-5, 600]$ kPa. Two individual sensors were connected to two individual measuring rings on each measurement location. At least 10 pipe diameters of straight pipes lead up the measurement locations. Sensor Total Error Band (TEB) accuracy was stated as $\pm 0.35\%$FS. The two turbine side pressures p_4 sensors had a range of $\Delta p \in [-100, 250]$ kPa, and a stated accuracy of 0.35% FS TEB. The two p_3 sensors had a stated accuracy of 0.35% FS TEB, and the range is thought to be $\Delta p \in [-5, 600]$ kPa. Two McCrometer Vcone differential pressure based measurement systems were used to measure different ranges of compressor mass flow ($W1$ and $W2$ in Fig. 1). For the small flow range, sensors with a range of $\pm$7kPa and a "Combined non-linearity & Hysteresis" accuracy of $\pm 0.08\%$ FS Best Straight Line (BSL) and "Temperature effect" of $\pm 1\%$ FS TEB are used. The range of the differential pressure sensors for the larger flow regime were $\pm$50kPa), but here the accuracy and temperature effect were stated as $\pm 0.08\%$ and $\pm 1\%$, respectively. The sensors were GE Druck sensors of series PMP4110. JAQUET T411-S5 tachometers were used to measure turbo shaft speed. The accuracy was stated to be $< 0.5\%$ FS, and a lower blade pass frequency of $f_{blade,min} = 3$kHz was stated.

(a) Gas stand room.

(b) Screw compressor room.

(c) Control room

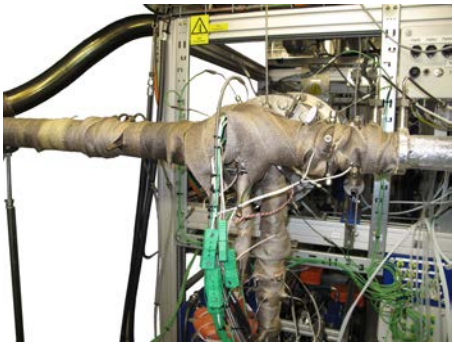

(d) Installation photo.

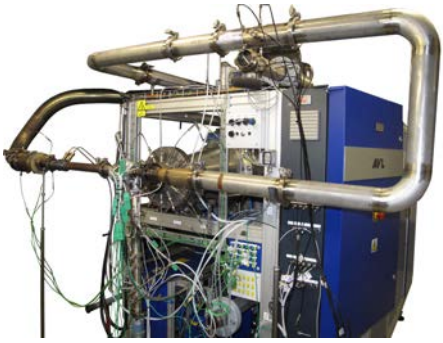

(e) Installation for pressurizing compressor inlet before insulation.

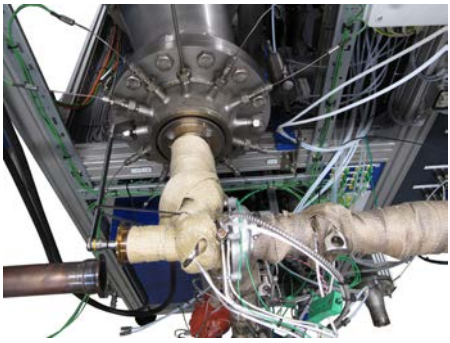

(f) Setup for zero turbo speed with typical insulation installed.

Figure 4.5: Photos from the measurements conducted in the Saab gas stand for Paper 5.

References

The *"(Cited on p. **7,8,12**)"* of the reference list indicates the pages within the introductory chapters of this compilation thesis, where the reference is used.

[1] M. Abidat, M. Hachemi, M.K. Hamidou, and N.C. Baines. Prediction of the steady and non-steady flow performance of a highly loaded mixed flow turbine. *Proc. of the IMechE, Part A: J. of Power and Energy*, 212:173–184, 1998. *(Cited on p. **27, 31**)*

[2] Habib Aghaali and Hans-Erik Ångström. Improving turbocharged engine simulation by including heat transfer in the turbocharger. In *SAE World Congr.*, Techn. Paper 2012-01-0703, 2012. *(Cited on p. **15, 16, 31**)*

[3] Markus Ammann. *Modellbasierte Regelung des Ladedrucks und der Abgasrückführung beim aufgeladenen PKW-Common-Rail-Dieselmotor*. PhD thesis 15166, ETH, Zürich, 2003. *(Cited on p. **15, 16, 28**)*

[4] Johannes Andersen, Erik Karlsson, and Anders Gawell. Variable turbine geometry on SI engines. In *SAE World Congr.*, Techn. Paper 2006-01-0020, Detroit, USA, March 2006. *(Cited on p. **14**)*

[5] Johannes Andersen, Fredrik Lindström, and Fredrik Westin. Surge definitions for radial compressors in automotive turbochargers. *SAE I.J. of Engines*, 1(1):218–231, 2009. *(Cited on p. **16, 18, 24, 25, 49**)*

[6] Per Andersson. *Air Charge Estimation in Turbocharged Spark Ignition Engines*. PhD thesis 989, Linköping University, 2005. *(Cited on p. **15, 28, 31, 32, 33, 44, 45, 48, 50**)*

[7] Steve Arnold. Turbocharging technologies to meet critital performance demands of ultra-low emissions diesel engines. In *SAE World Congr.*, Techn. Paper 2004-01-1359, 2004. *(Cited on p. **25**)*

[8] ASME. PTC 10-1997, Performance test code on compressors and exhausters. American Society of Mechanical Engineers, New York, 1997. *(Cited on p. **18, 52**)*

[9] Nicholas C. Baines. *Fundamentals of Turbocharging*. Concepts NREC, 1st edition, 2005. *(Cited on p. **4, 10, 13, 14, 30, 32, 33, 40**)*

[10] Nick Baines, Karl D. Wygant, and Antonis Dris. The analysis of heat transfer in automotive turbochargers. In *Proc. of ASME Turbo Expo*, GT2009-59353, June 2009. *(Cited on p. **15, 16**)*

[11] Nick Baines, Karl D. Wygant, and Antonis Dris. The analysis of heat transfer in automotive turbochargers. *Trans. of ASME, J. of Engineering for Gas Turbines and Power*, 132(4):1–8, 2010. *(Cited on p. **15, 21, 29**)*

[12] Rowland S. Benson. Nonsteady flow in a turbocharger nozzleless radial gas turbine. In *SAE*, Techn. Paper 740739, 1974. *(Cited on p. **27, 30**)*

[13] G. Benvenuto and U. Campora. Dynamic simulation of a high-performance sequentially turbocharged marine diesel engine. *I.J. of Engine Research*, 3(3):115–125, 2002. *(Cited on p. **22**)*

[14] Johan Bergström and Oskar Leufvén. Surge modeling and control of automotive turbochargers. Master's thesis LiTH-ISY-EX-3999, Linköping University, 2007. *(Cited on p. **7**)*

[15] Bjørnar Bøhagen and Jan Tommy Gravdahl. On active surge control of compressors using a mass flow observer. In *Proc. IEEE Conf. on Decision and Control*, volume 4, pages 3684–3689, Dec 2002. *(Cited on p. **28**)*

[16] Yurij G. Borila. A sequential turbocharging method for highly-rated truck diesel engines. In *SAE*, Techn. Paper 860074, 1988. *(Cited on p. **28**)*

[17] K.K. Botros. Transient phenomena in compressor stations during surge. *Trans. of ASME, J. of Engineering for Gas Turbines and Power*, (116):133–142, 1994. *(Cited on p. **38, 43**)*

[18] F. Bozza, V. De Bellis, S. Marelli, and M. Capobianco. 1D simulation and experimental analysis of a turbocharger compresor for automotive engines under unsteady flow conditions. In *SAE World Congr.*, Techn. Paper 2011-01-1147, 2011. *(Cited on p. **18**)*

[19] Julia H. Buckland. *Estimation Methods for Turbocharged Spark Ignition Engines*. PhD thesis, University of Michigan, 2009. *(Cited on p. **15, 30**)*

[20] P. M. Came and C. J. Robinson. Centrifugal compressor design. *Proc. of the IMechE, Part C: J. of Mechanical Engineering, Science*, 213(2), 1999. *(Cited on p. **11, 12, 13, 24**)*

[21] Marcello Canova. Development and validation of a control-oriented library for the simulation of automotive engines. *I.J. of Engine Research*, 5(3):219–228, 2004. *(Cited on p. **28**)*

[22] Marcello Canova, Fabio Chiara, Giorgio Rizzoni, and Yue-Yun Wang. Design and validation of a control-oriented model of a diesel engine with two-stage turbocharger. *SAE I.J. of Fuels and Lubricants*, 2(2):387–397, 2009. *(Cited on p. **31, 38, 43, 45**)*

[23] Marcello Canova, Junqiang Zhou, Lisa Fiorentini, Fabio Chiara, and Yue-Yun Wang. Model-based analysis and optimization of turbocharged diesel engines with a variable geometry compressor and turbine system. In *SAE World Congr.*, Techn. Paper 2012-01-0716, 2012. *(Cited on p. **13**)*

[24] Massimo Capobianco and Agostino Gambarotta. Variable geometry and waste-gated automotive turbochargers: Measurements and comparison of turbine performance. *Trans. of ASME, J. of Engineering for Gas Turbines and Power*, 114:553–560, 1992. *(Cited on p. **27, 31**)*

[25] Massimo Capobianco, Agostino Gambarotta, and Giovanni Cipolla. Effect of inlet pulsating pressure characteristics on turbine performance of an automotive wastegated turbocharger. In *SAE World Congr.*, Techn. Paper 900359, 1990. *(Cited on p. **17, 21, 22, 27, 30**)*

[26] Michael V. Casey and Thomas M. Fesich. On the efficiency of compressors with diabatic flows. In *Proc. of ASME Turbo Expo*, GT2009-59015, June 2009. *(Cited on p. **15, 16, 25**)*

[27] M.V. Casey and M. Schlegel. Estimation of the performance of turbocharger compressors at extremely low pressure ratios. *Proc. of the IMechE, Part A: J. of Power and Energy*, 224(2), 2010. *(Cited on p. **25, 26, 29, 39, 40, 41, 42**)*

[28] Kirby S. Chapman and Jacque Shultz. Guidelines for: Testing large-bore engine turbochargers. Technical report, The National Gas Machinery Laboratory, Kansas State University, 245 Levee Drive, 2003. *(Cited on p. **18**)*

[29] A. Chasse, P. Moulin, A. Albrecht, L. Fontvielle, A. Guinois, and L. Doléac. Double stage turbocharger control strategies development. In *SAE World Congr.*, Techn. Paper 2008-01-0988, 2008. *(Cited on p. **28**)*

[30] Colin D. Copeland, Ricardo Martinez-Botas, and Martin Seiler. Unsteady performance of a double entry turbocharger turbine with a comparison to steady flow conditions. In *Proc. of ASME Turbo Expo*, GT2008-50827, June 2008. *(Cited on p. **27**)*

[31] M. Cormerais, J.F. Hetet, P. Chesse, and A. Maiboom. Heat transfer analysis in a turbocharger compressor: modeling and experiments. In *SAE World Congr.*, Techn. Paper 2006-01-0023, Detroit, USA, March 2006. *(Cited on p. **16**)*

[32] Costall, McDavid, Martinez-Botaz, and Baines. Pulse performance modeling of a twin entry turbocharger turbine under full and and unequal admission. In *Proc. of ASME Turbo Expo*, GT2009-59406, June 2009. *(Cited on p. **22, 27, 28**)*

[33] Ivan Criscuolo, Oskar Leufvén, Andreas Thomasson, and Lars Eriksson. Model-based boost

pressure control with system voltage disturbance rejection. In *Proc. of IFAC World Congr.*, pages 5058–5063, 2011. *(Cited on p. **6**)*

[34] Bram de Jager. Rotating stall and surge control: A survey. In *Proc. IEEE Conf. on Decision and Control*, pages 1857–1862, Dec 1995. *(Cited on p. **23, 25, 38**)*

[35] R. Dehner, A. Selamet, P. Keller, and M Becker. Simulation of mild surge in a turbocharger compression system. In *SAE World Congr.*, Techn. Paper 2010-01-2142, 2010. *(Cited on p. **23, 24, 38, 39**)*

[36] Michael Deligant, Pierre Podevin, Georges Descombes, Lamquin Thierry, Vidal Fabrice, and Alexandre Marchal. Experimental study of turbocharger's performances at low speeds. In *Proc. ASME Int. Combustion Engine Division Fall Tech. Conf.*, ICEF2010-35071, pages 911–918, 2010. *(Cited on p. **17, 33**)*

[37] J.M. Desantes, B. Plá J.M. Luján, and J.A. Soler. Potential of using a nozzle at the compressor inlet of a high-speed direct-injection diesel engine. *J. of Applied Thermal Engineering*, 225:178–189, 2011. *(Cited on p. **13**)*

[38] S.L. Dixon. *Fluid Mechanics and Thermodynamics of Turbomachinery.* Butterworth-Heinemann, 4th edition, 1998. *(Cited on p. **4, 10, 15, 18, 39, 40, 41**)*

[39] Thomas Eidenböck, Karl Mayr, Werner Neuhauser, and Peter Staub. The new BMW six-cylinder diesel engine with three turbochargers part 1: Drive unit and turbocharger system. *MTZ*, 73(1):18–24, 2012. *(Cited on p. **28**)*

[40] Jamil El Hadef, Guillaume Colin, Yann Chamaillard, and Vincent Talon. Physical-based algorithms for interpolation and extrapolation of turbocharger data maps. *SAE I.J. of Engines*, 5(2), May 2012. *(Cited on p. **43, 45**)*

[41] Jamil El Hadef, Guillaume Colin, Vincent Talon, and Yann Chamaillard. New physics-based turbocharger data-maps extrapolation algorithms: Validation on a spark-ignited engine. In *IFAC ECOSM*, pages 213–220, 2012. *(Cited on p. **23, 31, 33, 43, 45**)*

[42] Abraham Engeda, Yanbae Kim, Ronald Aungier, and Gregory Direnzi. The inlet flow structure of a centrifugal compressor stage and its influence on the compressor performance. *J. of Fluids Engineering*, 125:779–785, 2003. *(Cited on p. **11, 41**)*

[43] Lars Eriksson. Mean value models for exhaust system temperatures. *SAE I.J. of Engines*, 111(3), Sept 2002. *(Cited on p. **15, 28**)*

[44] Lars Eriksson. Modeling and control of turbocharged SI and DI engines. *Oil & Gas Science and Technology - Rev. IFP*, 62(4):523–538, 2007. *(Cited on p. **31, 32, 43**)*

[45] Lars Eriksson, Tobias Lindell, Oskar Leufvén, and Andreas Thomasson. Scalable component-based modeling for optimizing engines with supercharging, E-boost and turbocompound concepts. *SAE I.J. of Engines*, 5(2):579–595, May 2012. *(Cited on p. **6, 28**)*

[46] Lars Eriksson, Tobias Lindell, Oskar Leufvén, and Andreas Thomasson. Scalable component-based modeling for optimizing engines with supercharging, e-boost and turbocompound concepts. In *SAE World Congr.*, Techn. Paper 2012-01-0713, 2012. *(Cited on p. **6**)*

[47] Lars Eriksson and Lars Nielsen. *Modeling and control of engines and drivelines.* Vehicular systems, ISY, Linköping Institute of Technology, 2009. *(Cited on p. **32, 41, 45**)*

[48] Lars Eriksson, Lars Nielsen, Jan Brugård, Johan Bergström, Fredrik Pettersson, and Per Andersson. Modeling of a turbocharged SI engine. *Annual Reviews in Control*, 26(1):129–137, 2002. *(Cited on p. **28, 31, 32, 34, 44, 45**)*

[49] Olof Erlandsson. *Thermodynamic Simulation of HCCI Engine Systems.* PhD thesis 989, Department of Heat and Power Engineering, Lund Institute of Technology, 2002. *(Cited on p. **26**)*

[50] Dominic Evans and Andrew Ward. Minimising turbocharger whoosh noise for diesel powertrains. In *SAE World Congr.*, Techn. Paper 2005-01-2485, 2005. *(Cited on p. **24**)*

[51] D.A. Fink, N.A. Cumpsty, and Edward M. Greitzer. Surge dynamics in a free-spool centrifugal compressor system. *J. of Turbomachinery*, 114:321–332, Apr 1992. *(Cited on p. **23, 24, 25**)*

[52] F.B. Fisher. Application of map width enhancement devices to turbocharger compressor stages. In *SAE*, Techn. Paper 880794, 1988. *(Cited on p. **13**)*

[53] Oscar Flärdh and Jonas Mårtensson. Analysis of a quasi-steady extension to the turbine model in mean value engine models. In *SAE World Congr.*, Techn. Paper 2010-01-1191, 2010. *(Cited on p. **27**)*

[54] J. Galindo, F. Arnau, A. Tiseira, R. Lang, H. Lahjaily, and T. Gimenes. Measurement and modeling of compressor surge on engine test bench for different intake line configurations. In

SAE World Congr., Techn. Paper 2011-01-0370, 2011. *(Cited on p. **23, 24, 38**)*

[55] J. Galindo, H. Climent, C. Guardiola, and J. Domenech. Strategies for improving the mode transition in a sequential parallel turbocharged automotive diesel engine. *I.J. of Automotive Technology*, 10(2):141–149, 2009. *(Cited on p. **28**)*

[56] J. Galindo, H. Climent, C. Guardiola, and A. Tiseira. Assessment of a sequantially turbocharged diesel engine on real-life driving cycles. *I.J. of Vehicle Design*, 49(1/2/3):214–234, 2009. *(Cited on p. **4**)*

[57] J. Galindo, J.M. Luján, C. Guardiola, and G.S. Lapuente. A method for data inconsistency checking in compressor and variable-geometry turbine maps. *Proc. of the IMechE, Part D: J. of Automobile Engineering*, 220(3):1465–1473, 2006. *(Cited on p. **11, 14, 23, 27**)*

[58] J. Galindo, J.R. Serrano, H. Climent, and A. Tiseira. Experiments and modelling of surge in small centrifugal compressor for automotive engines. *J. of Experimental Thermal and Fluid Science*, 32(3):818–826, 2008. *(Cited on p. **23, 37, 38, 39**)*

[59] J. Galindo, J.R. Serrano, C. Guardiola, and C. Cervelló. Surge limit definition in a specific test bench for the characterization of automotive turbochargers. *J. of Experimental Thermal and Fluid Science*, 30(5):449–462, 2006. *(Cited on p. **18, 24, 25**)*

[60] J. Galindo, J.R. Serrano, X. Margot, A. Tiseira, N. Schorn, and H. Kindl. Potential of flow pre-whirl at the compressor inlet of automotive engine turbochargers to enlarge surge margin and overcome packaging limitations. *I.J. of Heat and Fluid Flow*, 28(3):374–387, 2007. *(Cited on p. **40, 41**)*

[61] J. Galindo, A. Tiseira, F.J. Arnau, and R. Lang. On-engine measurement of turbocharger surge limit. *Experimental Techniques*, 37(1):47–54, 2013. *(Cited on p. **24, 25**)*

[62] S. García-Nieto, M. Martínez, X. Blasco, and J. Sanchis. Nonlinear predictive control based on local model networks for air management in diesel engines. *Control Engineering Practice*, 16(12):1399–1413, 2008. *(Cited on p. **31**)*

[63] P. Gautier, A. Albrecht, A. Chasse, P. Moulin, A. Pagot, L. Fontvieille, and D. Issartel. A simulation study of the impact of lp egr on a two-stage turbocharged diesel engine. *Oil & Gas Science and Technology - Rev. IFP*, 64(3):361–379, 2009. *(Cited on p. **28**)*

[64] Jan Tommy Gravdahl and Olav Egeland. Speed and surge control for a low order centrifugal compressor model. IEEE Int. Conf. on Control Applications, pages 344–349, 1997. *(Cited on p. **39, 40, 41**)*

[65] Jan Tommy Gravdahl and Olav Egeland. Centrifugal compressor surge and speed control. *IEEE Trans. on Control Systems Technology*, 7(5):567–579, Sept 1999. *(Cited on p. **22, 38, 39, 40, 41**)*

[66] Jan Tommy Gravdahl, Olav Egeland, and Svein Ove Vatland. Active surge control of centrifugal compressors using drive torque. volume 2 of *Proc. IEEE Conf. on Decision and Control*, 2001. *(Cited on p. **38, 44**)*

[67] Jan Tommy Gravdahl, Frank Willems, Bram de Jager, and Olav Egeland. Modeling for surge control of centrifugal compressors: comparison with experiment. In *Proc. IEEE Conf. on Decision and Control*, volume 2, pages 1341–1346, Dec 2000. *(Cited on p. **11, 24, 28, 38, 41**)*

[68] Jan Tommy Gravdahl, Frank Willems, Bram de Jager, and Olav Egeland. Modeling of surge in free-spool centrifugal compressors: experimental validation. *J. of Propulsion and Power*, 20(5):849–857, Sept-Oct 2004. *(Cited on p. **24, 38**)*

[69] Edward M. Greitzer. The stability of pumping systems - The 1980 Freeman Scholar Lecture. *J. of Fluids Engineering*, 103:193–242, 1981. *(Cited on p. **23, 24, 25, 37**)*

[70] Panagiotis Grigoriadis. *Experimentelle Erfassung und Simulation instantionärer Verdichterphänomene bei Turboladern von Fahrzeugmotoren.* PhD thesis, Technischen Universität Berlin, 2008. *(Cited on p. **22, 24, 25, 38**)*

[71] Fahua Gu, Abraham Engeda, Mike Cave, and Jean-Luc Di Liberti. A numerical investigation on the volute/diffuser interaction due to the axial distortion at the impeller exit. *J. of Fluids Engineering*, 123(3):475–483, 2001. *(Cited on p. **29**)*

[72] L. Guzzella and A. Amstutz. Control of diesel engines. *Control Systems Magazine, IEEE*, 18(5):53–71, Oct 1998. *(Cited on p. **32, 33, 34, 44, 45, 48**)*

[73] K. E. Hansen, P. Jørgensen, and P. S. Larsen. Experimental and theoretical study of surge in a small centrifugal compressor. *J. of Fluids Engineering*, 103:391–395, 1981. *(Cited on p. **23, 24, 38, 43**)*

[74] Fredrik Hellström. *Numerical computations of the unsteady flow in turbochargers*. PhD thesis, KTH, Fluid Physics, 2010. *(Cited on p. **25, 29, 41**)*

[75] Elbert Hendricks. A compact, comprehensive model of a large turbocharged, two-stroke diesel engine. Techn. Paper 861190, 1986. *(Cited on p. **28**)*

[76] Elbert Hendricks. Isothermal vs. adiabatic mean value SI engine models. In *3rd IFAC Workshop, Advances in Automotive Control, Preprints, Karlsruhe, Germany*, pages 373–378, March 2001. *(Cited on p. **28**)*

[77] F. Herbst, C.-P. Stöber-Schmidt, P. Eilts, T. Sextro, J. Kammeyer, C. Natkaniec, J. Seume, D. Porzig, and H. Schwarze. The potential of variable compressor geometry for highly boosted gasoline engines. In *SAE World Congr.*, Techn. Paper 2011-01-0376, 2011. *(Cited on p. **17**)*

[78] John B. Heywood. *Internal Combustion Engine Fundamentals*. McGraw-Hill series in mechanical engineering. McGraw-Hill, 1988. *(Cited on p. **3, 30**)*

[79] Hermann Hiereth and Peter Prenninger. *Charging the Internal Combustion Engine*. Springer Wien NewYork, 2007. *(Cited on p. **10, 12, 13, 14, 26, 30, 39**)*

[80] Ulrich Hopmann and Marcelo C. Algrain. Diesel engine electric turbo compound technology. In *SAE World Congr.*, Techn. Paper 2003-01-2294, 2003. *(Cited on p. **13**)*

[81] Xiao Hu and Patrik B. Lawless. Predictions of on-engine efficiency for the radial turbine of a pulse turbocharged engine. In *SAE World Congr.*, Techn. Paper 2001-01-1238, 2001. *(Cited on p. **27**)*

[82] K.A.R. Ismail, C.V.A.G. Rosolen, F.J. Benevenuto, and D. Lucato. Small radial compressors: Aerodynamic design and analysis. *I.J. of Rotating Machinery*, pages 189–200, 1998. *(Cited on p. **12, 41**)*

[83] J.-P. Jensen, A.F. Kristensen, S.C. Sorenson, N. Houbak, and E. Hendricks. Mean value modeling of a small turbocharged diesel engine. In *SAE World Congr.*, Techn. Paper 910070, Feb 1991. *(Cited on p. **28, 31, 32, 43, 45**)*

[84] Wei Jiang, Jamil Khan, and Roger A. Dougal. Dynamic centrifugal compressor model for system simulation. *J. of Power Sources*, 158(2):1333–1343, 2006. *(Cited on p. **41, 42**)*

[85] Merten Jung. *Mean-Value Modelling and Robust Control of the Airpath of a Turbocharged Diesel Engine*. PhD thesis, Sidney Sussex College, Department of Engineering, University of Cambridge, 2003. *(Cited on p. **18, 27, 28**)*

[86] Merten Jung, Richard G. Ford, Keith Glover, Nick Collings, Urs Christen, and Michael J. Watts. Parametrization and transient validation of a variable geometry turbocharger for mean-value modeling at low and medium speed-load points. In *Powertrain and Fluid Systems, Conference and Exhibition*, Techn. Paper 2002-01-2729, San Diego, California, USA, October 2002. *(Cited on p. **16, 18**)*

[87] N. Karamanis and R.F. Martinez-Botas. Mixed-flow turbines for automotive turbochargers: steady and unsteady performance. *I.J. of Engine Research*, 3(3):127–138, 2002. *(Cited on p. **27, 28**)*

[88] Y. Kim, A. Engeda, R. Aungier, and G. Direnzi. The influence of inlet flow distortion on the performance of a centrifugal compressor and the development of an improved inlet using numerical simulations. *Proc. of the IMechE, Part D: J. of Automobile Engineering*, 215, 2001. *(Cited on p. **22, 24**)*

[89] P. A. Konstantinidis, G. C. Koltsakis, and A. M. Stamatelos. Transient heat transfer modelling in automotive exhaust systems. *Proc. of the IMechE, Part C: J. of Mechanical Engineering, Science*, 211(1), 1997. *(Cited on p. **15**)*

[90] Eric Krivitzky and Louis Larosiliere. Aero design challenges in wide-operability turbocharger centrifugal compressors. In *SAE World Congr.*, Techn. Paper 2012-01-0710, 2012. *(Cited on p. **23, 41**)*

[91] Thierry Lamquin and Kostandin Gjika. Power losses identification on turbocharger hydrodynamic bearing systems: test and prediction. In *Proc. of ASME Turbo Expo*, GT2009-59599, June 2009. *(Cited on p. **17**)*

[92] Per-Inge Larsson, Fredrik Westin, Johannes Andersen, Joachim Vetter, and Alberto Zumeta. Efficient turbo charger testing. *MTZ*, 70(07-08):16–21, 2009. *(Cited on p. **56**)*

[93] B. Lee, Z. Filipi, D. Assanis, and D. Jung. Simulation-based assessment of various dual-stage boosting systems in terms of performance and fuel economy improvements. In *SAE World Congr.*, Techn. Paper 2009-01-1471, 2009. *(Cited on p. **4**)*

[94] Oskar Leufvén. Compressor modeling for control of automotive two stage turbocharg-

ers. Licenciate thesis, Division of Vehicular Systems, Department of Electrical Engineering, Linköping University, 2010. LiU-TEK-LIC-2010:32, Thesis No. 1463. *(Cited on p. **7**)*

[95] Oskar Leufvén and Lars Eriksson. Time to surge concept and surge control for acceleration performance. In *Proc. of IFAC World Congr.*, pages 2063–2068, 2008. *(Cited on p. **5**)*

[96] Oskar Leufvén and Lars Eriksson. Engine test bench turbo mapping. In *SAE World Congr.*, Techn. Paper 2010-01-1232, 2010. *(Cited on p. **5**)*

[97] Oskar Leufvén and Lars Eriksson. Surge and choke capable compressor model. In *Proc. of IFAC World Congr.*, pages 10653–10658, 2011. *(Cited on p. **5, 6**)*

[98] Oskar Leufvén and Lars Eriksson. Investigation of compressor correction quantities for automotive applications. *I.J. of Engine Research*, 13(6):588–606, December 2012. *(Cited on p. **5**)*

[99] Oskar Leufvén and Lars Eriksson. Measurement, analysis and modeling of centrifugal compressor flow for low pressure ratios. *Submitted to I.J. of Engine Research*, Under review. *(Cited on p. **6**)*

[100] Oskar Leufvén and Lars Eriksson. A surge and choke capable compressor flow model - validation and extrapolation capability. *Submitted to Control Engineering Practice*, Under review. *(Cited on p. **5**)*

[101] R. I. Lewis. *Turbomachinery Performance Analysis*. Arnold, 1996. *(Cited on p. **10, 18, 41**)*

[102] Per Erik Lindahl and William Sandqvist. *Mätgivare, mätning av mekaniska storheter och temperatur*. Studentlitteratur, 1996. *(Cited on p. **49**)*

[103] J. Macek, O. Vitek, and Z. Zak. Calibration and results of a radial turbine 1-D model with distributed parameters. In *SAE World Congr.*, Techn. Paper 2011-01-1146, 2011. *(Cited on p. **17, 29**)*

[104] J. Macek and O. Vítek. Simulation of pulsating flow unsteady operation of a turbocharger radial turbine. In *SAE World Congr.*, Techn. Paper 2008-01-0295, 2008. *(Cited on p. **15, 27**)*

[105] V. Macián, J. M. Luján, V. Bermúdez, and C. Guardiola. Exhaust pressure pulsation observation from turbocharger instantaneous speed measurement. *Measurement, Science and Technology*, 15(6):1185–1194, June 2004. *(Cited on p. **28**)*

[106] Silvia Marelli, Chiara Carraro, and Massimo Capobianco. Effect of pulsating flow characteristics on performance and surge limit of automotive turbocharger compressors. *SAE I.J. of Engines*, 5:596–601, 2012. *(Cited on p. **24, 25**)*

[107] Guillaume Martin, Vincent Talon, Pascal Higelin, Alain Charlet, and Christian Caillol. Implementing turbomachinery physics into data map-based turbocharger models. *SAE I.J. of Engines*, 2(1):211–229, 2009. *(Cited on p. **14, 22, 43, 45**)*

[108] J.R. McBride, P.W. Husak, J.A. Lockwood, and K.E. Nietering. High frequency measurements of pressure and temperature fluctuations in an automotive exhaust system during steady state and transient driving conditions. In *SAE World Congr.*, Techn. Paper 2001-01-0227, 2001. *(Cited on p. **27**)*

[109] Shishir Menon, Anthony Furman, and Michael Krok. Detection of surge precursors in locomotive turbocharger. In *Industrial Technology, 2006. ICIT 2006. IEEE International Conference on*, pages 3067–3071, Dec 2006. *(Cited on p. **18**)*

[110] R.B. Montgomery. Viscosity and thermal conductivity of air and diffusivity of water vapor in air. *J. of Meteorology*, 4:193–196, Dec 1947. *(Cited on p. **17**)*

[111] F.K. Moore and E.M. Greitzer. A theory of post-stall transients in axial compression systems: Part i - development of equations. *Trans. of ASME, J. of Engineering for Gas Turbines and Power*, (108):68–76, 1986. *(Cited on p. **37, 42**)*

[112] P. Moraal and I. Kolmanovsky. Turbocharger modeling for automotive control applications. In *SAE World Congr.*, Techn. Paper 1999-01-0908, March 1999. *(Cited on p. **16, 27, 31, 32, 44**)*

[113] Sayyed Mostafa Motavalli, Ali Hajilouy-Benisi, and Mahdi Nili-Ahmadabadi. Experimental and theoretical investigation of centrifugal compressor performance characteristics. In *Proc. of ASME Turbo Expo*, GT2008-50939, June 2008. *(Cited on p. **41**)*

[114] Matthias Mrosek and Rolf Isermann. On the parametrisation of turbocharger power and heat transfer models. In *IFAC AAC*, 2010. *(Cited on p. **15, 17, 33, 35**)*

[115] Matthias Mrosek, Sebastian Zahn, and Rolf Isermann. Parameter estimation for physical

based air path models of turbocharged diesel engines – an experience based guidance. *SAE I.J. of Engines*, 2(2):570–583, 2009. *(Cited on p. **51**)*

[116] M. Müller, S. Sumser, P. Fledersbacher, K. Rößler, K. Fieweger, and H.J. Bauer. Using the centrifugal compressor as a cold-air turbine. In *Int. conf. on turbochargers and turbocharging*, London, 2005. *(Cited on p. **26, 39**)*

[117] Martin Müller, Elbert Hendricks, and Spencer C. Sorenson. Mean value modelling of turbocharged spark ignition engines. In *SAE World Congr.*, Techn. Paper 980784, Detroit, USA, 1998. *(Cited on p. **40, 43**)*

[118] J. Nitta, A. Minato, and N. Shimazaki. Performance evaluation of three-stage turbocharging system for heavy-duty diesel engine. In *SAE World Congr.*, Techn. Paper 2011-01-0374, 2011. *(Cited on p. **28**)*

[119] Mattias Nyberg and Thomas Stutte. Model based diagnosis of the air path of an automotive diesel engine. *Control Engineering Practice*, 12(5):513–525, 2004. *(Cited on p. **28**)*

[120] W. Oakes, P. Lawless, and S. Fleeter. High-speed centrifugal compressor instabilities during speed transients. *J. of Aerospace Engineering*, 17(3):106–112, 2004. *(Cited on p. **25**)*

[121] Jan-Ola Olsson. Boost limitation in a torque based engine management system. In *IFAC Symposium*, Advances in Automotive Control, pages 609–616, 2007. *(Cited on p. **28**)*

[122] Rabih Omran, Rafic Younes, and Jean-Claude Champoussin. Optimal control of a variable geometry turbocharged diesel engine using neural networks: Applications on the ETC test cycle. *IEEE Trans. on Control Systems Technology*, 17(2):380–393, March 2009. *(Cited on p. **31, 33, 43, 46**)*

[123] J. Panting, K.R. Pullen, and R.F. Martinez-Botas. Turbocharger motor-generator for improvement of transient performance in an internal combustion engine. *Proc. of the IMechE, Part D: J. of Automobile Engineering*, 215:369–383, 2001. *(Cited on p. **15, 27**)*

[124] F. Payri, J. Galindo, H. Climent, and C. Guardiola. Measurement of the oil consumption of an automotive turbocharger. *Experimental Techniques*, 29(5):25–27, 2005. *(Cited on p. **15**)*

[125] Pentronic. Pentronics temperaturhandbok 1, 1997. *(Cited on p. **51**)*

[126] Alexandros Plianos and Richard Stobart. Modeling and control of diesel engines equipped with a two-stage turbo-system. In *SAE World Congr.*, Techn. Paper 2008-01-1018, 2008. *(Cited on p. **32, 43, 45**)*

[127] Helmut Pucher, Torsten Eggert, and Björn Schenk. Experimentelle Entwicklungswerkzeuge für Turbolader von Fahrzeugmotoren. 6. Aufladetechnische Konferenz, Dresden, pages 227–240, Oct 1997. *(Cited on p. **38**)*

[128] Xuwen Qiu, Dave Japikse, Jinhui Zhao, and Mark R. Anderson. Analysis and validation of a unified slip factor model for impellers at design and off-design conditions. In *GT2010-22164*, Proc. of ASME Turbo Expo, June 2010. *(Cited on p. **41**)*

[129] C.D. Rakopoulos, C.N. Michos, and E.G. Giakoumis. Study of the transient behavior of turbocharged diesel engines including compressor surging using a linearized quasi-steady analysis. In *SAE World Congr. Modeling of SI and Diesel Engine 2005 (SP-1969)*, Techn. Paper 2005-01-0225, 2005. *(Cited on p. **23, 38, 43, 45**)*

[130] K.G. Rochford. Series turbocharging - a requirement for high specific output, vehicular diesel engines. In *SAE*, Techn. Paper 790067, 1979. *(Cited on p. **11**)*

[131] Alessandro Romagnoli and Richard Martinez-Botaz. Heat transfer on a turbocharger under constant load points. In *Proc. of ASME Turbo Expo*, GT2009-59618, June 2009. *(Cited on p. **17**)*

[132] J.A. Röth and L. Guzzella. Modelling engine and exhaust temperatures of a mono-fuelled turbocharged compressed-natural-gas engine during warm-up. *Proc. of the IMechE, Part D: J. of Automobile Engineering*, 224(1), 2010. *(Cited on p. **15**)*

[133] SAE standard. J1826 – Turbocharger Gas Stand Test Code, 1995. *(Cited on p. **18**)*

[134] SAE standard. J922 – Turbocharger Nomenclature and Terminology, 1995. *(Cited on p. **18**)*

[135] J.Vicente Salcedo, Emanuele Pieroni, Emilio Pérez, Xavier Blasco, Miguel Martínez, and J. Vicente García. Real-time control and simulation of a non-linear model for air management in a turbocharged diesel engine. In *FISITA World Automotive Congress*, F2004-F373, 2004. *(Cited on p. **31**)*

[136] T. Sato, J. M. Oh, and A. Engeda. Experimental and numerical investigation of the flow in a vaneless diffuser of a centrifugal compressor stage. part 1: Experimental investigation. *Proc. of the IMechE, Part C: J. of Mechanical Engineering, Science*, 219(10), Sept 2005. *(Cited*

on p. ***41)***

[137] S. Schmitt, W. Schmid, G. Hertweck, and M. Schlegl. Hochpräzise Messungen der Reibleistungen von Abgasturboladern. In *Supercharging Conference, Dresden Germany*, pages 185–206, 2007. *(Cited on p.* ***14, 17, 33****)*

[138] Marc Sens, Jonas Nickel, Panagiotis Grigoriadis, and Helmut Pucher. Influence of sensors and measurement system configuration on mapping and the use of turbochargers in the vehicle. In *SAE World Congr.*, Techn. Paper 2006-01-3391, Detroit, USA, March 2006. *(Cited on p.* ***18, 22****)*

[139] Rodolphe Sepulchre and Petar Kokotovic. Shape signifiers for control of a low-order compressor model. *Automatic Control, IEEE Trans. on*, 43(11):1643–1648, Nov 1998. *(Cited on p.* ***43****)*

[140] J.R. Serrano, F.J. Arnau, V. Dolz, A. Tiseira, and C. Cervelló. A model of turbocharger radial turbines appropriate to be used in zero- and one-dimensional gas dynamics codes for internal combustion engines modelling. *I.J. of Energy Conversion and Management*, 49(12):3729–3745, 2008. *(Cited on p.* ***27, 30****)*

[141] J.R. Serrano, V. Dolz, A. Tisiera, and A. Páez. Influence of environmental conditions and thermodynamic considerations in the calculation of turbochargers efficiency. In *SAE World Congr.*, Techn. Paper 2009-01-1468, 2009. *(Cited on p.* ***17****)*

[142] J.R. Serrano, C. Guardiola, V. Dolz, A. Tiseira, and C. Cervelló. Experimental study of the turbine inlet gas temperature influence on turbocharger performance. In *SAE World Congr.*, Techn. Paper 2007-01-1559, Detroit, USA, 2007. *(Cited on p.* ***16****)*

[143] J.R. Serrano, B. Tormos, K.L. Gargar, and F. Bouffaud. Study of the effects on turbocharger performance generated by the presence of foreign objects at the compressor intake. *Experimental Techniques*, pages no–no, 2011. *(Cited on p.* ***22****)*

[144] S. Shaaban and J. Seume. Impact of turbocharger non-adibatic operation on engine volumetric efficency and turbo lag. *I.J. of Rotating Machinery*, 5, 2012. *(Cited on p.* ***15****)*

[145] Sameh Shaaban. *Experimental Investigation and Extended Simulation of Turbocharger Non-adiabatic Performance.* PhD thesis, Leibniz Universität Hannover, 2004. *(Cited on p.* ***11, 16, 21, 26, 27, 31, 39****)*

[146] Raef S. Shehata, Hussein A. Abdullah, and Fayez F.G. Areed. Variable structure surge control for constant speed centrifugal compressors. *Control Engineering Practice*, 17(7):815–833, 2009. *(Cited on p.* ***43****)*

[147] A. Sidorow, R. Isermann, F. Cianflone, and G. Landsmann. Model based fault detection of the air and exhaust path of diesel engines including turbocharger models. In *SAE World Congr.*, Techn. Paper 2011-01-0700, 2011. *(Cited on p.* ***15, 17, 18****)*

[148] C. H. Sieverding, T. Arts, R. Dénos, and J.-F. Brouckaert. Measurement techniques for unsteady flows in turbomachines. *Experiments in Fluids*, 28:285–321, 2000. *(Cited on p.* ***49****)*

[149] J.S. Simon, L. Valavani, A.H. Epstein, and Edward M. Greitzer. Evaluation of approaches to active compressor surge stabilization. *J. of Turbomachinery*, 115:57–67, Jan 1993. *(Cited on p.* ***23****)*

[150] Borislav Sirakov and Michael Casey. Evaluation of heat transfer effects on turbocharger performance. In *Proc. of ASME Turbo Expo*, GT2011-45887, June 2011. *(Cited on p.* ***16****)*

[151] Subenuka Sivagnanasundaram, Stephen Spence, Juliana Early, and Bahram Nikpour. An investigation of compressor map width enhancement and a detailed analysis of inducer flow field. *The Hong Kong Institution of Engineers Transaction*, 17(4):23–30, 2010. *(Cited on p.* ***13****)*

[152] A.A. Sokolov and S.T. Glad. Identifiability of turbocharged IC engine models. In *SAE World Congr.*, Techn. Paper 1999-01-0216, March 1999. *(Cited on p.* ***30, 45****)*

[153] Richard Stone. *Introduction to Internal Combistion Engines.* MacMillan London, 2nd edition, 1992. *(Cited on p.* ***3****)*

[154] Jan F. Suhrmann, Dieter Peitsch, Marc Gugau, Tom Heuer, and Uwe Tomm. Validation and development of loss models for small size radial turbines. In *GT2010-22666*, Proc. of ASME Turbo Expo, June 2010. *(Cited on p.* ***14, 30****)*

[155] E. Swain. Diesel engine transient performance prediction during sequential turbocharging operations. *Proc. of the IMechE, Part C: J. of Mechanical Engineering, Science*, pages 123–131, 1993. *(Cited on p.* ***31, 32****)*

[156] E. Swain. Improving a one-dimensional centrifugal compressor performance prediction method. *Proc. of the IMechE, Part A: J. of Power and Energy*, 219, 2005. *(Cited on p. **39**)*

[157] S. Szymko, N. R. McGlashan, R. Martinez-Botas, and K. R. Pullen. The development of a dynamometer for torque measurement of automotive turbocharger turbines. *Proc. of the IMechE, Part D: J. of Automobile Engineering*, 221(2):225–239, 2007. *(Cited on p. **22**)*

[158] M. Tancrez, J. Galindo, C. Guardiola, P. Fajardo, and O. Varnier. Turbine adapted maps for turbocharger engine matching. *J. of Experimental Thermal and Fluid Science*, 35(1):146–153, 2011. *(Cited on p. **31**)*

[159] X. Tauzia, J.F. Hetet, P. Chesse, G. Grosshans, and L. Mouillard. Computer aided study of the transient performances of a highly rated sequentially turbocharged marine diesel engine. *Proc. of the IMechE, Part A: J. of Power and Energy*, 212:185–196, 1998. *(Cited on p. **39**)*

[160] Edward S. Taylor. *Dimensional analysis for engineers*. Clarendon Press, Oxford, 1974. *(Cited on p. **18**)*

[161] G. Theotokatos and N.P. Kyrtatos. Diesel engine transient operation with turbocharger compressor surging. In *SAE World Congr.*, Techn. Paper 2001-01-1241, 2001. *(Cited on p. **38**)*

[162] Andreas Thomasson and Lars Eriksson. Model-based throttle control using static compensators and IMC based PID-design. In *IFAC ECOSM*, 2009. *(Cited on p. **28**)*

[163] Andreas Thomasson and Lars Eriksson. Modeling and control of co-surge in bi-turbo engines. In *Proc. of IFAC World Congr.*, pages 13010–13015, 2011. *(Cited on p. **39, 44**)*

[164] Andreas Thomasson, Lars Eriksson, Oskar Leufvén, and Per Andersson. Wastegate actuator modeling and model-based boost pressure control. In *IFAC ECOSM*, pages 87–94, 2009. *(Cited on p. **7, 28**)*

[165] Andreas Thomasson, Oskar Leufvén, Ivan Criscuolo, and Lars Eriksson. Modeling and validation of a boost pressure actuation system, for a series sequentially turbocharged SI engine. *Control Engineering Practice*, Accepted for publication, 2013. *(Cited on p. **6, 28**)*

[166] A.J. Torregrosa, J.R. Serrano, and J.A. Dopazo. Experiments on wave transmission and reflection by turbochargers in engine operating conditions. In *SAE World Congr.*, Techn. Paper 2006-01-0022, Detroit, USA, March 2006. *(Cited on p. **24**)*

[167] Johan Wahlström. *Control of EGR and VGT for Emission Control and Pumping Work Minimization in Diesel Engines*. PhD thesis, Linköping university, 2009. *(Cited on p. **28**)*

[168] Johan Wahlström and Lars Eriksson. Modelling diesel engines with a variable-geometry turbocharger and exhaust gas recirculation by optimization of model parameters for capturing non-linear system dynamics. *Proc. of the IMechE, Part D: J. of Automobile Engineering*, 225(7):960–986, 2011. *(Cited on p. **31, 44, 45**)*

[169] A.J. Ward-Smith. Critical flowmetering: The characteristics of cylindrical nozzles with sharp upstream edges. *I.J. of Heat and Fluid Flow*, 1(3):123–132, 1979. *(Cited on p. **30**)*

[170] N. Watson and M.S. Janota. *Turbocharging the internal combustion engine*. MacMillan London, 1982. *(Cited on p. **3, 4, 10, 11, 12, 13, 14, 15, 17, 22, 26, 27, 30, 32, 39, 40, 41**)*

[171] M.H. Westbrook and J.D. Turner. *Automotive sensors*. IOP Publishing, 1994. *(Cited on p. **49**)*

[172] Fredrik Westin. Accuracy of turbocharged SI-engine simulations. Licentiate thesis, Internal Combustion Engines, Department of Machine Design, Royal Institute of Technology, Stockholm, Sweden, 2002. *(Cited on p. **17, 26, 33**)*

[173] Fredrik Westin and Ragnar Burenius. Measurement of interstage losses of a twostage turbocharger system in a turbocharger test rig. In *SAE World Congr.*, Techn. Paper 2010-01-1221, 2010. *(Cited on p. **13, 24, 56**)*

[174] F.M White. *Fluid Mechanics*. McGraw-Hill, 2005. *(Cited on p. **18, 41**)*

[175] Frank Willems. Modeling and control of compressor flow instabilities. Report no. wfw 96.151, Faculty of Mechanical Engineering, Control Engineering Section, Eindhoven University of Technology, 1997. *(Cited on p. **11, 23, 25, 38**)*

[176] Frank Willems and Bram de Jager. Modeling and control of compressor flow instabilities. *Control Systems, IEEE*, 19(5):8–18, Oct 1999. *(Cited on p. **22, 23, 38**)*

[177] J. E. Ffowcs Williams and X. Y. Huang. Active stabilization of compressor surge. *Journal of Fluid Mechanics*, 204:245–262, 6 1989. *(Cited on p. **23, 43**)*

[178] D.E. Winterbone and R.J. Pearson. Turbocharger turbine performance under unsteady flow - a review of experimental results and proposed models. *Proc. of the IMechE, Part C: J. of Mechanical Engineering, Science*, pages 193–206, 1998. *(Cited on p. **27**)*

[179] A.M Wo and J.P. Bons. Flow physics leading to sytsem instability in a centrifugal pump. *J. of Turbomachinery*, 116:612–620, Oct 1994. *(Cited on p. **23**)*

[180] M. Yang, X Zheng, Y. Zhang, and Z Li. Improved performance model of turbocharger centrifugal compressor. In *Proc. of ASME Turbo Expo*, GT2008-50009, June 2008. *(Cited on p. **26, 42**)*

[181] Donghui Zhang, Jean-Luc Di Liberti, and Michael Cave. Blade thickness effect on impeller slip factor. In *Proc. of ASME Turbo Expo*, GT2010-22164, June 2010. *(Cited on p. **29**)*

[182] Zhe Zhang, Kangyao Deng, Zhenbiao Wang, and Xiangguo Zhu. Experimental study on the three-phase sequential turbocharging system with two unequal size turbochargers. *SAE I.J. of Fuels and Lubricants*, 1:1181–1186, 2008. *(Cited on p. **28**)*

[183] Karl Zinner. *Aufladung von Verbrennungsmotoren. Grundlagen, Berechnungen, Ausführungen*. Springer Verlag, 1985. *(Cited on p. **4, 10, 11**)*

Linköping studies in science and technology. Dissertations.
Division of Vehicular Systems
Department of Electrical Engineering
Linköping University

No. 1 Magnus Pettersson *Driveline Modeling and Control*, 1997

No. 2 Lars Eriksson *Spark Advance Modeling and Control*, 1999

No. 3 Mattias Nyberg *Model Based Fault Diagnosis: Methods, Theory, and Automotive Engine Applications*, 1999

No. 4 Erik Frisk *Residual Generation for Fault Diagnosis*, 2001

No. 5 Per Andersson *Air Charge Estimation in Turbocharged Spark Ignition Engines*, 2005

No. 6 Mattias Krysander *Design and Analysis of Diagnosis Systems Using Structural Methods*, 2006

No. 7 Jonas Biteus *Fault Isolation in Distributed Embedded Systems*, 2007

No. 8 Ylva Nilsson *Modelling for Fuel Optimal Control of a Variable Compression Engine*, 2007

No. 9 Markus Klein *Single-Zone Cylinder Pressure Modeling and Estimation for Heat Release Analysis of SI Engines*, 2007

No. 10 Anders Fröberg *Efficient Simulation and Optimal Control for Vehicle Propulsion*, 2008

No. 11 Per Öberg *A DAE Formulation for Multi-Zone Thermodynamic Models and its Application to CVCP Engines*, 2009

No. 12 Johan Wahlström *Control of EGR and VGT for Emission Control and Pumping Work Minimization in Diesel Engines*, 2009

No. 13 Anna Pernestål *Probabilistic Fault Diagnosis with Automotive Applications*, 2009

No. 14 Erik Hellström *Look-ahead Control of Heavy Vehicles*, 2010

No. 15 Erik Höckerdal *Model Error Compensation in ODE and DAE Estimators with Automotive Engine Applications*, 2011

No. 16 Carl Svärd, *Methods for Automated Design of Fault Detection and Isolation Systems with Automotive Applications*, 2012.